nature communications

Article

https://doi.org/10.1038/s41467-026-70349-8

Tudor domain-containing protein 9-targeting siRNA nanoparticles alleviate *Pseudomonas aeruginosa* lung injury in preclinical models by promoting neutrophil cuproptosis

Received: 20 May 2025

Accepted: 20 February 2026

Published online: 06 March 2026

Check for updates

Wei Zhang[1,2,8], Hui Li[3,8], Huayun Jia[4], Weixia Xuan[5], Lisha Ding[4], Zhenghong Tan[2,6], Qian Wu[7], Meiyun Zhao[2,6] & Xu Wu[2,6]

Pseudomonas aeruginosa pneumonia poses a significant therapeutic challenge. Nanoparticles serve as an effective tool for nucleic acid delivery to efficiently alleviate pneumonia. This study develops a hyaluronic acid (HA)-coated peptide nanoparticle system for targeted delivery of small interfering RNA (siRNA) against Tudor domain-containing protein 9 (*TDRD9*), identified via RNA sequencing of bronchoalveolar lavage fluid-derived neutrophils from 21 recruited patients (11 males/10 females). Adoptive transfer of TDRD9-silenced polymorphonuclear neutrophils into neutrophil-depleted male mice attenuates lung inflammation and edema. Mechanistically, TDRD9 suppresses neutrophil cuproptosis by upregulating programmed death ligand 1 (PD-L1) through interaction with CD80 to activate p38 mitogen-activated protein kinase (MAPK) signaling. HA-si-TDRD9 nanoparticles enhance neutrophil cuproptosis, reduce pulmonary neutrophil accumulation, and ameliorate lung injury via PD-L1/CD80/MAPK. Importantly, HA-si-TDRD9 nanoparticles reduce bacterial growth, apoptosis, and inflammation in human lung organoids. This work demonstrates that targeting *TDRD9* with siRNA nanoparticle platform presents a promising therapeutic strategy for treating bacterial lung injury.

Pseudomonas aeruginosa (PA), a ubiquitous and metabolically versatile Gram-negative bacterium, represents the predominant opportunistic pathogen in immunocompromised populations[1]. PA infections contribute substantially to global morbidity and mortality, clinically presenting as pneumonia, respiratory tract infections, sepsis, and surgical site complications[2]. PA colonization subverts host immune defenses through the secretion of virulence factors, biofilm formation, and quorum-sensing-mediated regulation[3,4]. Despite therapeutic

[1]Department of General Practice, the Second Affiliated Hospital, University of South China, Hengyang, China. [2]Hengyang Medical School, University of South China, Hengyang, China. [3]Department of Emergency, the Affiliated Nanhua Hospital, Hengyang Medical School, University of South China, Hengyang, China. [4]Biosafety Level 3 Laboratory, Hunan Province Center for Disease Control and Prevention, Changsha, China. [5]Department of Respiratory and Critical Care Medicine, Henan Provincial People's Hospital; People's Hospital of Zhengzhou University, Zhengzhou, China. [6]Pulmonary and Critical Care Medicine, the Second Affiliated Hospital, University of South China, Hengyang, China. [7]Institute of Human Virology, Zhongshan School of Medicine, and Key Laboratory of Tropical Disease Control of Ministry of Education, Sun Yat-sen University, Guangzhou, China. [8]These authors contributed equally: Wei Zhang, Hui Li.
e-mail: wx1048946906@126.com

advancements in recent years, the prevalence of multidrug-resistant PA strains compromises clinical outcomes[5]. Consequently, developing alternative or adjunctive therapeutic strategies to mitigate infection-associated morbidity remains an urgent priority.

During infection, PA triggers diverse modes of regulated cell death in host cells[6]. Neutrophils—the primary immune effectors recruited to infection sites—play critical roles in bacterial clearance during early inflammatory responses[7]. Emerging evidence identifies neutrophils as key targets of PA pathogenesis, with neutrophil dysfunction exacerbating host susceptibility to invasive infections[8]. PA orchestrates pathogenic strategies to induce neutrophil death, including promotion of NETosis (neutrophil extracellular trap formation)[9] and enhancement of caspase-1-dependent pyroptosis[10]. These findings collectively implicate neutrophil death modulation as a central virulence mechanism.

Cuproptosis, a novel copper-dependent programmed cell death pathway[11], involves cytotoxic copper accumulation that disrupts mitochondrial metabolism. Mechanistically, excessive intracellular copper binds to lipoylated enzymes in the tricarboxylic acid cycle, inducing mitochondrial proteotoxic stress through aggregation of iron-sulfur cluster proteins and subsequent loss of Fe-S-dependent enzyme activity. Recent studies correlate cuproptosis-related gene expression patterns with neutrophil infiltration dynamics[12,13], while neutrophil extracellular trap formation has been shown to suppress tumor cell cuproptosis[14]. Nevertheless, the role of neutrophil cuproptosis in PA infection pathogenesis remains unexplored.

RNA interference-based therapies, which selectively suppress target gene mRNA expression, demonstrate considerable potential for pneumonia treatment[15]. Nanoparticles (NPs) have emerged as robust vehicles for systemic and localized siRNA delivery, addressing inherent limitations of naked RNA therapeutics—including short plasma half-life, inefficient cellular uptake, and endosomal entrapment—while enhancing efficacy and minimizing off-target effects[16]. Notably, NP-mediated siRNA delivery systems exhibit intrinsic antibacterial properties capable of penetrating microbial biofilms[17,18]. However, the functional relevance of siRNA NPs in neutrophil-specific modulation during PA-induced pulmonary infection remains uncharacterized.

To address this gap, we identified Tudor domain-containing protein 9 (*TDRD9*) as significantly upregulated in pulmonary neutrophils from PA-infected mice using RNA sequencing in this study. While TDRD9 has been primarily characterized for its role in spermatogenesis[19], emerging clinical evidence links TDRD9 overexpression to pediatric bacterial pneumonia[20], chronic obstructive pulmonary disease, and community-acquired pneumonia[21]. This reinforces the understanding that *TDRD9* may act as a pathogenic factor in lung injury progression. We engineered a peptide-based siRNA NP platform to achieve TDRD9 knockdown and functional exploration. Our findings demonstrated that neutrophil-specific TDRD9 deletion potentiates cuproptosis, conferring protection against PA-induced pulmonary dysfunction in mice. Mechanistically, we delineated that TDRD9 silencing activates the PD-L1/CD80/MAPK signaling axis to drive pro-cuproptotic effects in neutrophils. Primary human lung organoids (HLOs) were cultured and differentiated from patient-derived adjacent non-cancerous tissues. Using the HLO cultures, it was observed that si-TDRD9 NPs alleviated bacterial growth and reduced cellular apoptosis. These results establish a foundational framework for TDRD9-targeted therapeutic strategies in PA pneumonia management.

Results

TDRD9 is upregulated in PA-induced pneumonia patients

Neutrophils, central effectors of innate immunity, play pivotal roles in PA-mediated lung injury[22], necessitating identification of pathogenic genes modulating neutrophil biology for therapeutic targeting. We performed RNA-seq on BALF-derived neutrophils isolated from control, non-PA pneumonia, and PA-induced pneumonia patients. Comparative analysis revealed extensive differential gene expression between Control and PA-pneumonia neutrophils (Fig. 1A). Subsequent stratification of pneumonia subgroups identified *PDE4D*, *TDRD9*, *SIGLEC14*, and *ITGA7* as markedly overexpressed in PA-pneumonia neutrophils versus non-PA pneumonia counterparts (Fig. 1B). qRT-PCR confirmed transcriptional upregulation of these candidates, with *TDRD9* demonstrating the most pronounced elevation in PA-pneumonia neutrophils (Fig. 1C). These findings indicate that *TDRD9* upregulation is associated with PA pneumonia development.

Neutrophilic TDRD9 is essential for mitigating post-infectious pneumonia in mouse models

To interrogate neutrophil-mediated pathobiology during PA lung infection, wild-type mice were intranasally inoculated with PA strain PAO1. BALF and lung tissues were harvested at 1-, 3-, and 7-day post-infection (Fig. 2A). PAO1 challenge induced progressive weight loss (Fig. 2B). Bacterial burden progressively increased in mouse lungs following PAO1 infection (Fig. 2C). PA-associated pneumonia is characterized by neutrophilic infiltration and protein-rich pulmonary edema[23,24]. Quantification of lung dry/wet weight ratios confirmed PAO1-driven pulmonary edema (Fig. 2D), while histopathological analysis via H&E staining revealed pronounced neutrophilic inflammation with elevated pathological scores (Fig. 2E). BALF cytokine profiling demonstrated elevated levels of TNF-α, IL-1β, and IL-6 (Fig. 2F), corroborating dysregulated inflammation. Flow cytometry revealed the dynamic recruitment of immune cells (Supplementary Fig. 1A–C). Notably, neutrophils peaked early (day 3) before declining in response to PA infection (Fig. 2G, H). Other examined immune cell populations remained relatively stable or exhibited opposite trends at days 1 and 3 post-infection (Fig. 2G, H, Supplementary Fig. 1B–D). Consequently, we selected day 3 post-PA infection for subsequent studies, as this point is characterized by a PA-specific pro-inflammatory environment and immune dysregulation.

Notably, PAO1 infection upregulated PDE4D, TDRD9, and ITGA7 expression in lung neutrophils, with TDRD9 showing the most robust induction (Fig. 3A, B). Given the critical role of neutrophil death in infection resolution[25], we assessed PAO1's impact on cell death pathways. Western blot analyses revealed suppression of apoptotic and pyroptotic markers (caspase family), reduced autophagic flux (decreased LC3-II, accumulated p62), and diminished disulfide death mediators (SLC7A11, GLUT1) in infected neutrophils (Supplementary Figs. 2A–C). Concurrently, ferroptosis was inhibited, evidenced by elevated GPX4, reduced ROS, and decreased Fe^{2+} (Supplementary Fig. 2D–F). Intriguingly, PAO1 also modulated cuproptosis—a copper-dependent cell death pathway implicated in lung pathogenesis[26]. Infected neutrophils exhibited upregulated dihydrolipoamide S-acetyltransferase (DLAT), ferredoxin1 (FDX1), lipoyl synthase (LIAS), ATPase copper transporter 7A and 7B (ATP7A/B), but downregulated solute carrier family 31 member 1(SLC31A1) and p53 (Fig. 3C). IF confirmed enhanced co-localization of neutrophil marker Ly6G with DLAT and FDX1 in PAO1-infected lungs (Fig. 3D), implicating TDRD9 in cuproptosis suppression during neutrophilic PA infection.

To functionally validate TDRD9's role, circulating neutrophils were depleted via anti-Ly6G antibody 48 h pre-PAO1 challenge (Fig. 4A). While neutrophil ablation did not alter baseline weight or lung integrity in non-infected mice, it exacerbated PAO1-induced weight loss and pulmonary damage (Fig. 4B–F). Strikingly, adoptive transfer of sh-TDRD9-transducted PMNs attenuated PAO1-driven pathology, including reduced bacterial burden, edema resolution, decreased neutrophilic infiltration, and diminished BALF cytokines (Fig. 4B–F). These findings establish TDRD9 as a critical regulator of neutrophil cuproptosis and lung injury during PA infection.

TDRD9 knockdown potentiates cuproptosis in human neutrophils

To investigate TDRD9's regulatory role in neutrophil cuproptosis, we established an in vitro model using human peripheral blood neutrophils and employed the copper ionophore ES to induce cuproptosis while modulating TDRD9 expression. Dose-response analysis via CCK-8 assay revealed progressive reduction in neutrophil viability with escalating ES concentrations (Fig. 5A). Subsequent experiments utilized 10 μM ES for 24 h, a regimen that significantly impaired viability with or without PAO1 treatment (Fig. 5B). PAO1 infection alone did not compromise neutrophil viability. PAO1 infection upregulated DLAT, FDX1, LIAS, ATP7A, and ATP7B while downregulating SLC31A1 and p53 in neutrophil lysates—a pattern reversed by ES treatment (Fig. 5C). Notably, PAO1 infection robustly induced TDRD9 expression (Fig. 5D), which correlated positively with DLAT, FDX1, LIAS, ATP7A/B and inversely with SLC31A1 and p53 (Fig. 5E), suggesting TDRD9 as a negative regulator of cuproptosis during PA infection.

To functionally validate this, we transducted neutrophils with sh-TDRD9 or oe-TDRD9 lentivirus. Transduction of sh-TDRD9 effectively suppressed TDRD9 expression, whereas oe-TDRD9 achieved overexpression (Supplementary Fig. 3A, B). TDRD9 knockdown reduced neutrophil viability, an effect partially rescued by the cuproptosis inhibitor tetrathiomolybdate but unaffected by inhibitors of ferroptosis (ferrostatin-1), apoptosis (Z-VAD-FMK), necroptosis (necrosulfonamide), or autophagy (3-MA) (Fig. 5F). In PAO1/ES-co-treated neutrophils, TDRD9 knockdown reduced bacterial burden (Fig. 5G). TDRD9 knockdown further diminished viability, while TDRD9 overexpression conferred resistance to ES cytotoxicity (Fig. 5H). TDRD9 knockdown increased PAO1-downregulated p53 levels in culture medium (Fig. 5I). Correspondingly, TDRD9 depletion reversed PAO1-induced upregulation of DLAT, FDX1, LIAS, ATP7A/B and restored SLC31A1/p53 levels, mimicking ES-driven cuproptosis. Conversely, TDRD9 overexpression antagonized ES-mediated cuproptotic signaling (Fig. 5J). These data establish TDRD9 as a critical suppressor of

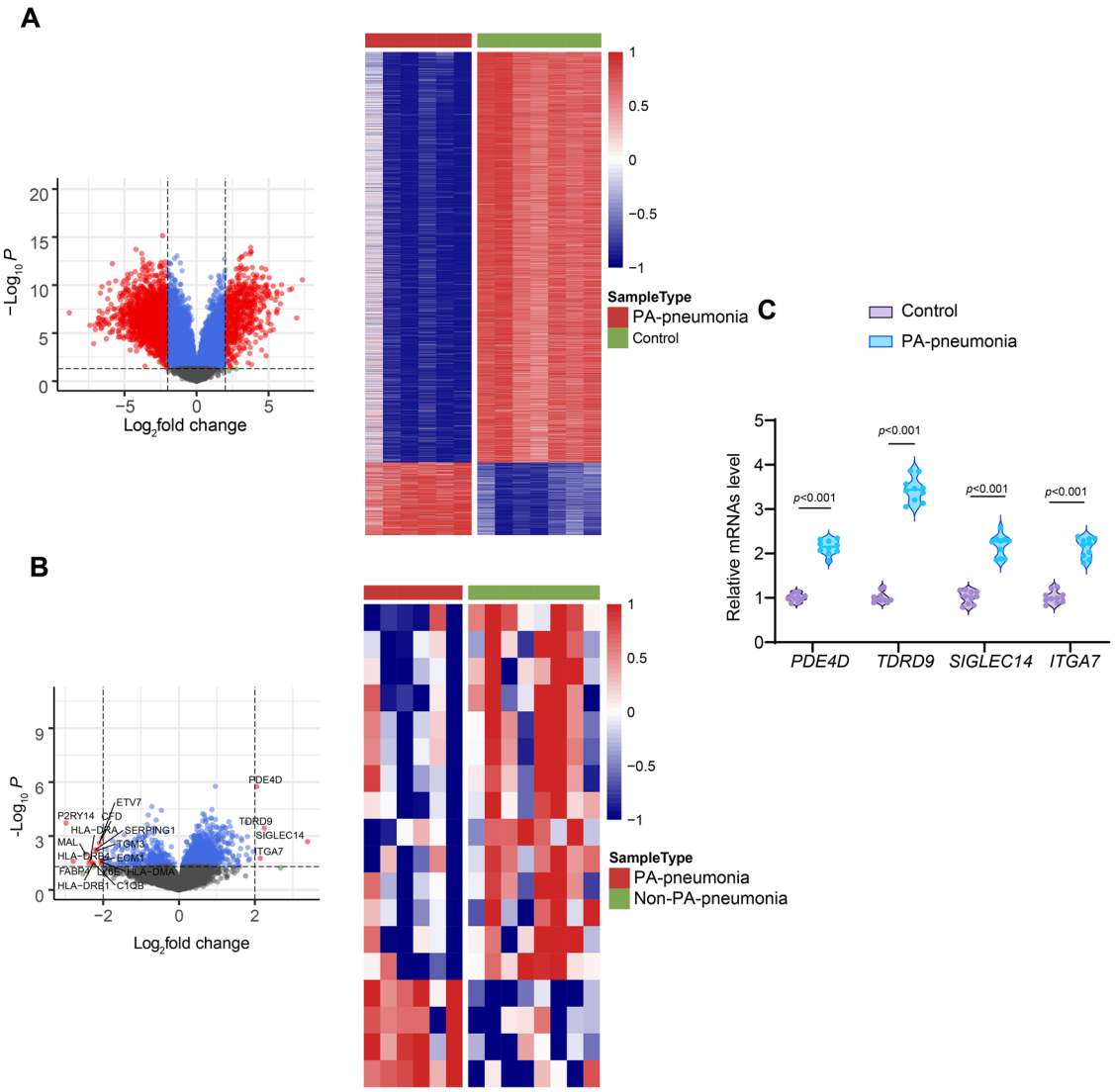

Fig. 1 | Transcriptomic profiling of differentially expressed genes in pneumonia patients. A Volcano plot and hierarchical clustering heatmap of differentially expressed genes (DEGs) between neutrophils from Control and *Pseudomonas aeruginosa* (PA)-pneumonia neutrophils. **B** Volcano plot and hierarchical clustering heatmap of DEGs between non-PA-pneumonia and PA-pneumonia neutrophils. **C** Male C57BL/6 mice received 50 μL of bacterial suspension of PA strain PAO1 (OD_{600} = 0.6; 7×10^6 CFU/mL in 0.9% sterile saline) via oropharyngeal intratracheal instillation. Control mice received an equal volume of sterile saline. Quantitative real-time PCR validation of upregulated genes (phosphodiesterase 4D [*PDE4D*], Tudor domain-containing protein 9 [*TDRD9*], sialic acid-binding Ig-like lectin 14 [*SIGLEC14*], integrin subunit alpha 7 [*ITGA7*]) in PA-pneumonia neutrophils versus Control. $n = 10$ mice per group. Data represent median ± interquartile range (IQR), and analyzed by two-sided *t*-test (**C**). Source data are provided as a Source Data file.

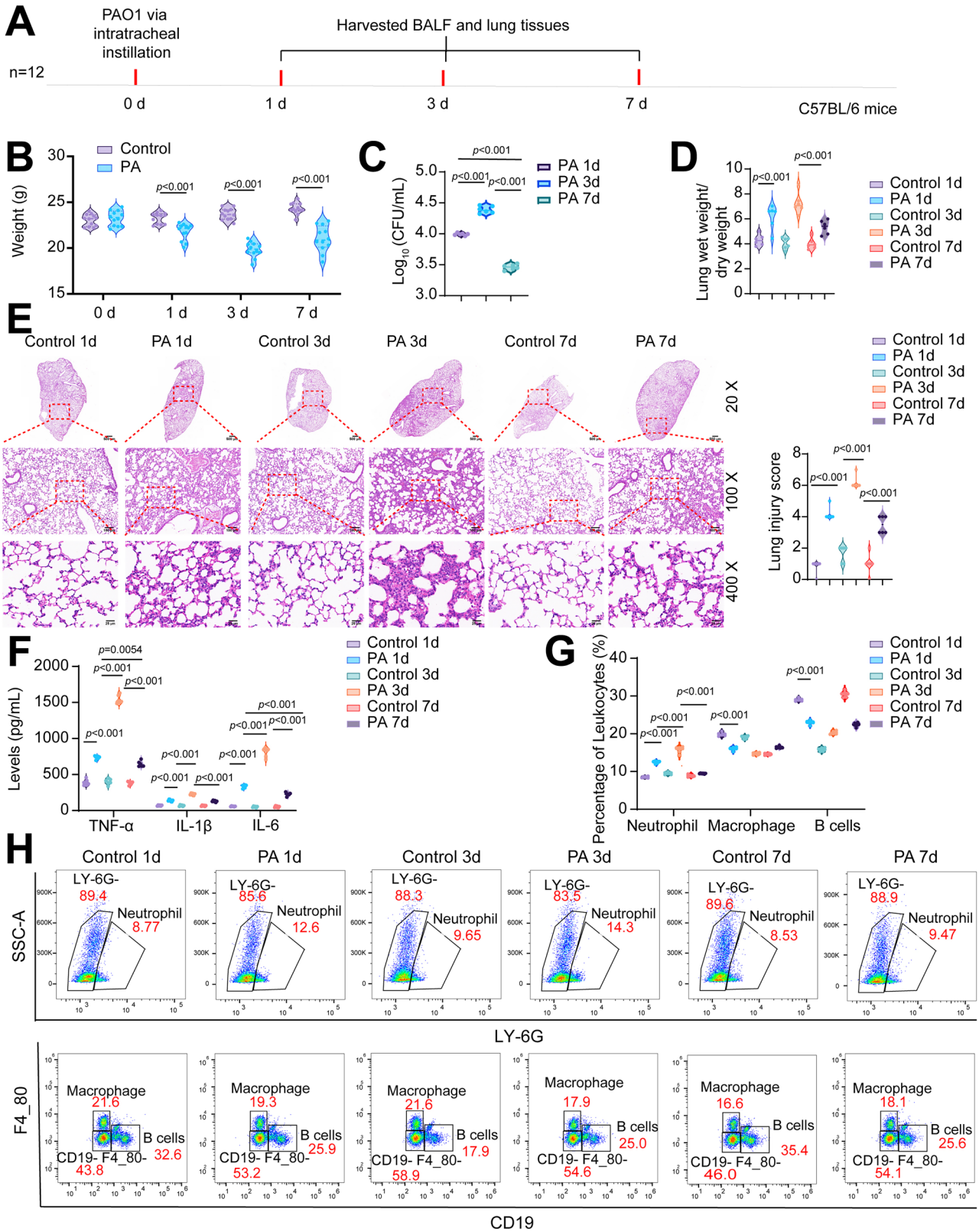

neutrophil cuproptosis, with its expression dictating cellular resilience to copper toxicity during PA infection.

RNA-seq identifies PD-L1/CD80/MAPK as key TDRD9-associated signaling nodes

To elucidate the mechanism underlying TDRD9-mediated regulation of neutrophil cuproptosis, we performed RNA-seq on PAO1-exposed human peripheral blood neutrophils following TDRD9 knockdown. Principal component analysis (PCA) confirmed distinct transcriptional profiles between sh-TDRD9 and sh-NC groups (Fig. 6A). Differential gene expression analysis identified 249 significantly altered transcripts, including 34 upregulated and 215 downregulated genes (Fig. 6B, C). Strikingly, *CD274* (encoding programmed cell death-ligand 1 [PD-L1]) emerged as a downregulated candidate in TDRD9-depleted

Fig. 2 | *Pseudomonas aeruginosa* (PA) induces lung injury in mice. A An experimental flowchart illustrating male C57BL/6 mice were intranasally inoculated with 50 μL of bacterial suspension of PA strain PAO1 (OD_{600} = 0.6; 7×10^6 CFU/mL in 0.9% sterile saline). Bronchoalveolar lavage fluid (BALF) and lung tissues were then harvested at 1-, 3-, and 7-day post-infection. **B** Body weight trajectories of mice over 7 days post-PAO1 infection. *n* = 12 mice per group. **C** Quantitative analysis of colony-forming unit (CFU) in lung tissues. n = 6 mice per group. **D** Quantification of pulmonary edema via lung dry-to-wet weight ratios. *n* = 6 mice per group. **E** Histopathological assessment of PAO1-induced lung injury by hematoxylin and eosin (HE) staining. Scale bar: 500 μm (top), 100 μm (middle), 25 μm (bottom). *n* = 6 mice per group. **F** Proinflammatory cytokine levels (tumor necrosis factor-alpha [TNF-α], interleukin-1 beta [IL-1β], and IL-6) in BALF measured by enzyme-linked immunosorbent assay (ELISA). *n* = 6 mice per group. **G**, **H** Flow cytometric quantification of neutrophils, macrophages, and B cells in lung tissues post-PAO1 infection. *n* = 6 mice per group. Data represent median ± interquartile range (IQR), and analyzed by two-sided two-way ANOVA with Tukey's multiple comparisons test (**B**), or two-sided one-way ANOVA with Tukey's multiple comparisons test (**C**–**G**). Source data are provided as a Source Data file.

neutrophils under PAO1 challenge. PD-L1 has been mechanistically linked to cuproptosis regulation. Elevated intracellular copper induces concurrent cuproptosis and PD-L1 upregulation in malignancies[27,28]. Anti-PD-L1 immunotherapy potentiates copper-dependent tumor cell death[29]. *CD274* suppression enhances tumor cell susceptibility to cuproptosis[30]. Sepsis-induced myocardial injury involves PD-L1/cuproptosis gene co-dysregulation[31]. These parallels suggest PD-L1 may serve as a TDRD9 effector in neutrophil copper homeostasis. GO enrichment analysis revealed DEGs were predominantly enriched in biological processes, including inflammatory response and positive regulation of MAPK cascade, cellular components, such as platelet alpha granule lumen, and molecular functions like acetylcholine-gated ion channel activity (Fig. 6D). Notably, PD-L1 is a known modulator of MAPK signaling[32], which itself regulates cuproptosis through FDX1 transcriptional control and protein stabilization[33–35]. PPI network analysis via STRING further identified PD-L1 (*CD274*) as a hub interacting with CD80 (Fig. 6E)—a ligand–receptor pair critical for immune checkpoint regulation[36]. Collectively, these data position the PD-L1/CD80/MAPK axis as a central pathway through which TDRD9 governs neutrophil cuproptosis during PA infection.

TDRD9 governs neutrophil cuproptosis via the PD-L1/CD80/MAPK signaling axis

To functionally validate the PD-L1/CD80/MAPK pathway as a downstream mediator of TDRD9-regulated cuproptosis, we interrogated molecular interactions in neutrophils co-treated with PAO1 and ES. Combined PAO1/ES exposure upregulated TDRD9, PD-L1, CD80, and phosphorylated p38 MAPK (p-p38), whereas TDRD9 knockdown suppressed these markers (Supplementary Fig. 4A, B). Rescue experiments demonstrated that PD-L1 overexpression in TDRD9-depleted neutrophils promoted bacterial growth (Fig. 7A), concurrently restoring PD-L1, CD80, and p-p38 levels (Fig. 7B, C), rescuing TDRD9 knockdown-induced viability loss (Fig. 7D), and reversing cuproptosis-related protein expression (Fig. 7E, F). These findings position PD-L1 as a critical effector of TDRD9-mediated p38 MAPK activation and cuproptosis suppression.

Mechanistic dissection revealed that PD-L1 overexpression alone elevated PD-L1, CD80, and p-p38 levels, whereas CD80 knockdown abrogated these effects (Fig. 7G, H). Functionally, PD-L1 overexpression enhanced neutrophil viability and anti-cuproptotic protein signatures, while CD80 depletion counteracted these effects (Fig. 7I–K). Co-IP confirmed direct PD-L1-CD80 interaction (Fig. 7L), establishing their cooperative role in signaling. MAPK activation using agonist U-46199 mitigated CD80 knockdown outcomes and mirrored PD-L1 overexpression outcomes—inducing p-p38 levels (Supplementary Fig. 4C, D), aggravating bacterial load (Fig. S4E), rescuing neutrophil viability (Supplementary Fig. 4F), upregulating DLAT/FDX1/LIAS/ATP7A/B, and suppressing SLC31A1/p53 (Supplementary Fig. 4G, H). These findings confirm PD-L1/CD80/MAPK's centrality in TDRD9-mediated cuproptosis.

Synthesis and functional validation of HA-si-TDRD9 NPs

Self-assembled siRNA NPs were synthesized through non-covalent complexation of p5RHH peptide with siRNA in HBSS buffer. To enhance cellular uptake, NPs were surface-functionalized with HA, a CD44-targeting ligand[37]. DLS revealed average hydrodynamic diameters of 321.0 ± 37.1 nm for HA-si-NC NPs (control) and 330.3 ± 42.1 nm for HA-si-TDRD9 NPs (Supplementary Fig. 5A). TEM confirmed spherical morphology and uniform size distribution, demonstrating that TDRD9 siRNA encapsulation does not alter nanoparticle architecture under the tested conditions (Supplementary Fig. 5B). Functional efficacy was assessed in human peripheral blood neutrophils. HA-si-TDRD9 NPs (0.01–0.2 μM) exhibited minimal cytotoxicity in untreated cells but induced dose-dependent viability reduction in PAO1-infected neutrophils, with 0.1 μM selected for subsequent experiments (Supplementary Fig. 5C, D). Cellular uptake analyses via IF and flow cytometry demonstrated superior internalization of Cy5.5-labeled HA-si-TDRD9 NPs compared to uncoated counterparts (Supplementary Fig. 5E, F). This enhancement was attributed to HA[38,39], as CD44 blockade significantly reduced NP uptake (Supplementary Fig. 5G). Consistent with improved delivery, HA-coated NPs achieved more potent *TDRD9* knockdown in neutrophils, as validated by qRT-PCR (Supplementary Fig. 5H).

HA-si-TDRD9 NPs potentiate neutrophil cuproptosis via PD-L1/CD80/MAPK signaling

To delineate the mechanistic role of HA-si-TDRD9 NPs in modulating neutrophil cuproptosis, we assessed molecular and functional outcomes under PA infection. In neutrophils co-treated with PAO1 and ES, HA-si-TDRD9 NPs suppressed TDRD9 expression and correspondingly downregulated PD-L1, CD80, and p-p38 (Supplementary Figs. 6A, B). HA-si-TDRD9 NPs also mitigated PAO1/ES-induced bacterial burden (Supplementary Fig. 6C). This suppression synergized with PAO1/ES to exacerbate neutrophil viability loss (Supplementary Fig. 6D) and cuproptosis induction, as evidenced by reduced DLAT, FDX1, LIAS, ATP7A/B, and elevated SLC31A1/p53 levels (Supplementary Fig. 6E). Further interrogation revealed that PD-L1 overexpression in HA-si-TDRD9 NP-treated cells restored PD-L1/CD80/p-p38 expression, while p38 inhibition (SB203580) selectively abrogated p-p38 without affecting upstream regulators (Supplementary Fig. 7A–B). Functionally, PD-L1 overexpression exacerbated bacterial load (Supplementary Fig. 7C), while attenuating HA-si-TDRD9 NP-driven viability loss and cuproptosis, whereas SB203580 reversed these effects (Supplementary Figs. 7D–F). These data establish HA-si-TDRD9 NPs as potent inducers of neutrophil cuproptosis during PA infection, operating through PD-L1/CD80/MAPK inactivation.

HA-si-TDRD9 NPs mitigate PA-induced lung injury

To evaluate the beneficial effects of HA-si-TDRD9 NPs in vivo, animals received intravenous administration of 0.1 μmol (low-dose) or 0.2 μmol (high-dose) HA-si-TDRD9 NPs before and after PAO1 challenge (Fig. 8A, Supplementary Fig. 8A). Compared to the HA-si-NC NPs-treated group, HA-si-TDRD9 NPs did not induce significant changes in body weight (Fig. 8B, Supplementary Fig. 8B). HA-si-TDRD9 NPs attenuated pulmonary bacterial load induced by PAO1 infection compared to HA-si-NC NPs-treated mice (Fig. 8C, Supplementary Fig. 8C). HA-si-TDRD9 NPs significantly attenuated pulmonary edema, as evidenced by reduced lung wet/dry weight ratios (Fig. 8D, Supplementary Fig. 8D). Furthermore, these nanoparticles markedly decreased cytokine levels (TNF-α, IL-1β, IL-6) in BALF (Fig. 8E, Supplementary Fig. 8E).

https://doi.org/10.1038/s41467-026-70349-8

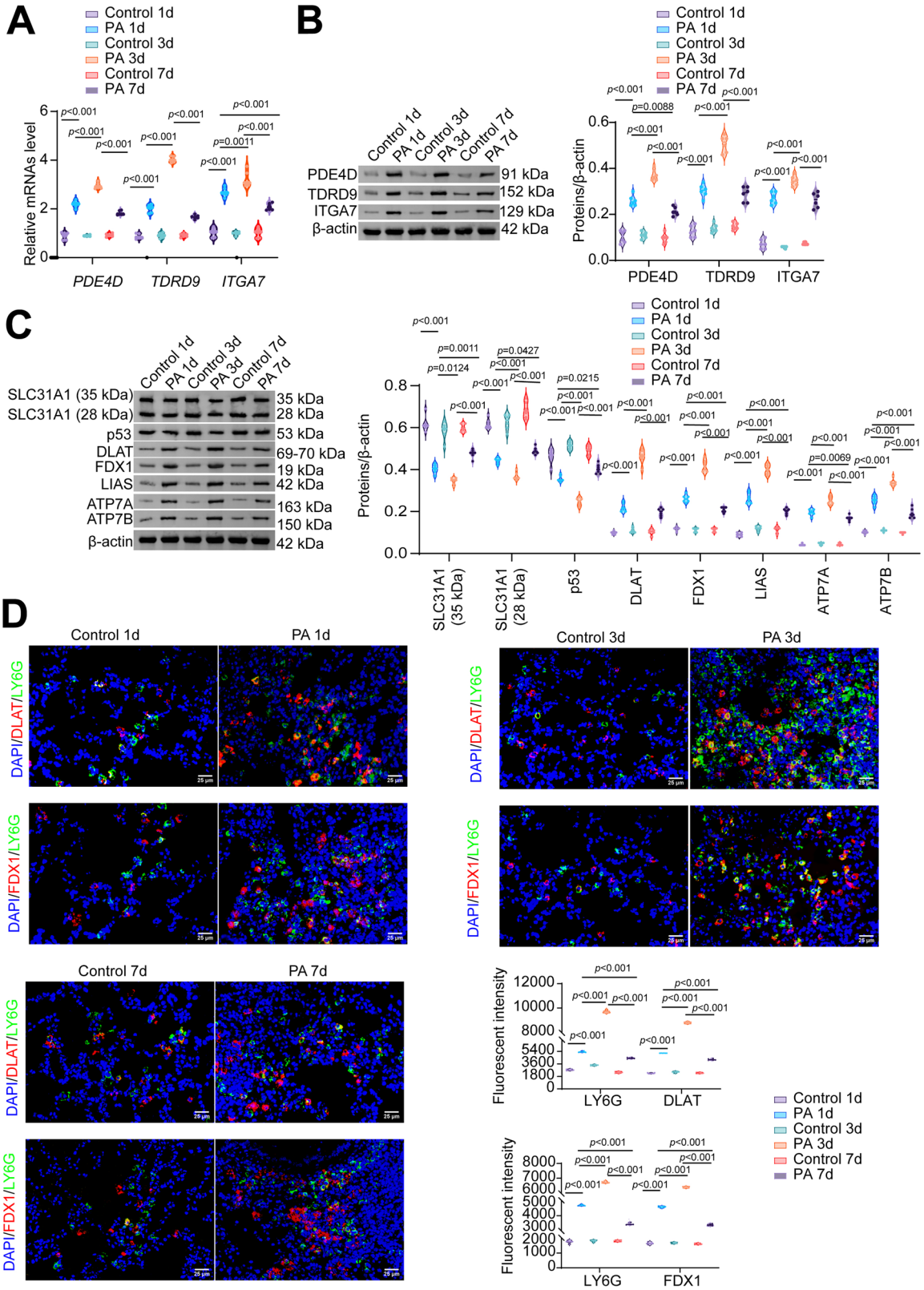

HE staining confirmed substantially reduced inflammatory infiltration and lower histopathological scores in HA-si-TDRD9 NPs-treated lung tissues (Fig. 8F, Supplementary Fig. 8F). Stained sections of hepatic and renal tissues from PA-infected or healthy mice demonstrated absence of significant necrosis or fibrosis in hepatic tissues across all mouse groups, with no vacuolar degeneration observed in renal tubular epithelial cells and intact glomerular structures (Supplementary Fig. S9A-C), indicating that HA-si-TDRD9 NPs did not induce substantial hepatorenal toxicity.

Neutrophils isolated from lung tissues demonstrated that HA-si-TDRD9 NPs downregulated expression of TDRD9, PD-L1, CD80, p-p38, and copper toxicity-associated proteins (DLAT, FDX1, LIAS, ATP7A/B), while upregulating SLC31A1 and p53 (Fig. 8G–I, Supplementary Fig. 8G–I). Dose-dependent efficacy was observed, with a high dose of

https://doi.org/10.1038/s41467-026-70349-8

Fig. 3 | *Pseudomonas aeruginosa* (PA) suppresses neutrophil cuproptosis in mouse lungs. Male C57BL/6 mice were intranasally inoculated with 50 μL of bacterial suspension of PA strain PAO1 (OD_{600} = 0.6; 7×10^6 CFU/mL in 0.9% sterile saline) for 1, 3, and 7 days. **A** Quantitative real-time PCR quantification of phosphodiesterase 4D (*PDE4D*), Tudor domain-containing protein 9 (*TDRD9*), and integrin subunit alpha 7 (*ITGA7*) in lung neutrophils. $n = 6$. mice per group. **B** Western blot analysis of PDE4D, TDRD9, and ITGA7 expression in lung neutrophils. $n = 6$ mice per group. **C** Western blot profiling of cuproptosis-related proteins (dihydrolipoamide S-acetyltransferase [DLAT], ferredoxin 1 [FDX1], lipoic acid synthetase [LIAS], copper-transporting ATPase A/B [ATP7A/B], solute carrier family 31 member 1 [SLC31A1], and tumor protein p53 [p53]) in neutrophils. $n = 6$ mice per group. **D** Immunofluorescence (IF) staining demonstrating co-localization of neutrophil marker LY6G (green) with Fe-S cluster proteins DLAT and FDX1 (red) in lung tissues. Nuclei were counterstained with DAPI (blue). Scale bar: 25 μm. $n = 6$ mice per group. Data represent median ± interquartile range (IQR), and analyzed by two-sided one-way ANOVA with Tukey's multiple comparisons test (**A**–**D**). Source data are provided as a Source Data file.

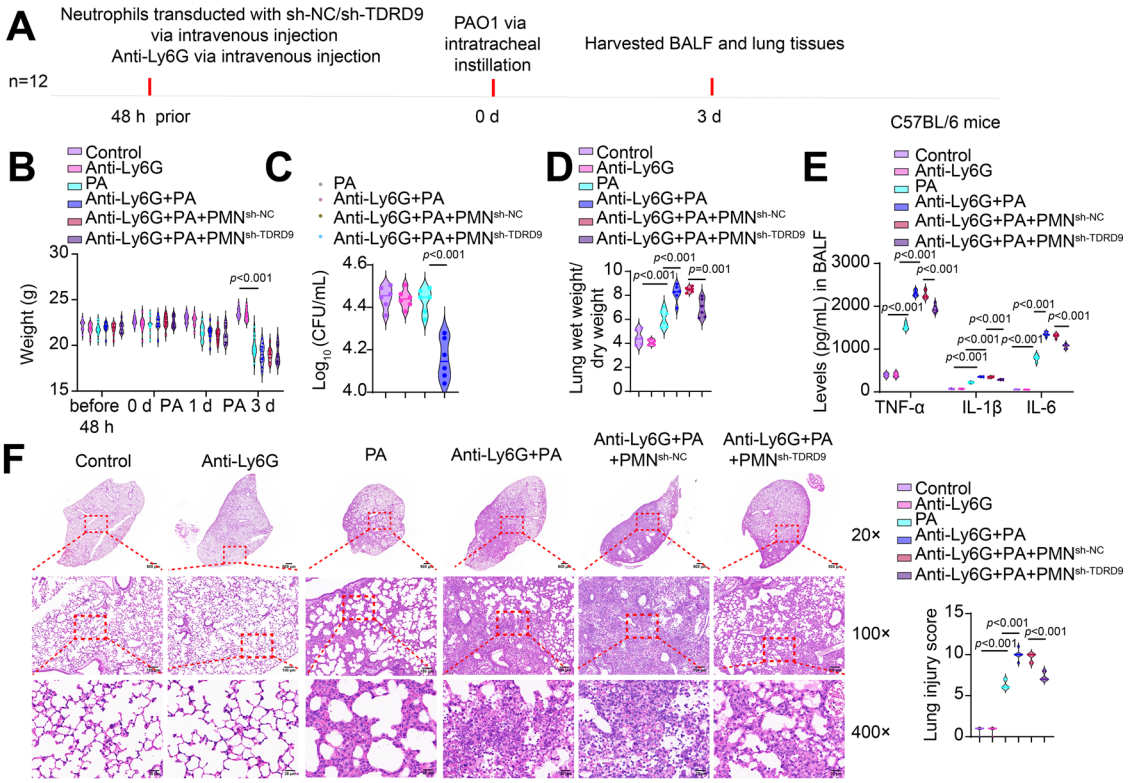

Fig. 4 | Neutrophil-specific Tudor domain-containing protein 9 (TDRD9) depletion attenuates *Pseudomonas aeruginosa* (PA)-induced pneumonia. A An experimental flowchart illustrating that male C57BL/6 mice were intravenously administered 50 μg anti-Ly6G antibody and intravenously injected with neutrophils (1×10^6 cells/mouse) 48 h prior to PA strain PAO1 (OD_{600} = 0.6; 7×10^6 CFU/mL in 0.9% sterile saline) infection. Neutrophils were pre-transducted with lentiviral-based short hairpin RNA (shRNA) knocking down *TDRD9* (sh-TDRD9) or corresponding negative control vectors (sh-NC). **B** Body weight changes in mice over 3 days post-PAO1 infection. $n = 12$ mice per group. **C** Quantitative analysis of colony-forming unit (CFU) in lung tissues. $n = 6$ mice per group. **D** Lung dry-to-wet weight ratios evaluating edema severity. $n = 6$ mice per group. **E** Bronchoalveolar lavage fluid (BALF) cytokine levels (tumor necrosis factor-alpha [TNF-α], interleukin-1 beta [IL-1β], and IL-6) were quantified by enzyme-linked immunosorbent assay (ELISA). $n = 6$ mice per group. **F** Hematoxylin and eosin (HE) staining reveals inflammatory damage in lung tissues. Scale bar: 500 μm (top), 100 μm (middle), 25 μm (bottom). $n = 6$ mice per group. Data represent median ± interquartile range (IQR), and analyzed by two-sided two-way ANOVA with Tukey's multiple comparisons test (**B**), or two-sided one-way ANOVA with Tukey's multiple comparisons test (**C**–**F**). Source data are provided as a Source Data file.

HA-si-TDRD9 NPs demonstrating superior therapeutic outcomes. These findings collectively establish HA-si-TDRD9 NPs as a promising strategy for mitigating lung injury during PA infection.

HA-si-TDRD9 NPs reduce HLO susceptibility to PA infection

Recent advancements in stem cell research enable the in vitro cultivation of 3D organoids that recapitulate the structural, biological, and functional characteristics of native tissues[40]. Using a HLO host model, we validated the protective effects of HA-si-TDRD9 NPs against PA infection. Spherical 3D HLO structures were successfully established in Matrigel, exhibiting progressive growth over 7 days (Fig. 9A). HE staining confirmed that HLOs retained vacuolated morphology consistent with native lung tissue (Fig. 9B). IHC verified the expression of stem/progenitor markers (Ki67, NKX2.1, SOX9) in HLOs (Fig. 9C). PA-challenged HLOs displayed marked structural damage, which was attenuated by HA-si-TDRD9 NPs (Fig. 9D). HA-si-TDRD9 significantly suppressed bacterial proliferation in HLOs (Fig. 9E) and reduced PA-induced upregulation of TDRD9 mRNA and protein levels. Concurrently, HA-si-TDRD9 downregulated PA-triggered PD-L1, CD80, and p-p38 expression (Fig. 9F–G). TUNEL assays revealed increased apoptotic cells and elevated cleaved caspase-3/8/9 levels in PA-exposed HLOs, both of which were reversed by HA-si-TDRD9 (Fig. 9H, I). Furthermore, HA-si-TDRD9 reduced PA-induced inflammatory cytokine levels (TNF-α, IL-1β, IL-6) in HLOs (Fig. 9J). Collectively, these data demonstrate that HA-si-TDRD9 NPs mitigate HLO susceptibility to PA infection.

Discussion

PA infection contributes to pulmonary dysfunction in patients, a critical factor in respiratory failure and mortality[41]. Developing potential therapeutic strategies to improve clinical outcomes in pneumonia remains imperative. In this study, transcriptomic analysis of human

https://doi.org/10.1038/s41467-026-70349-8

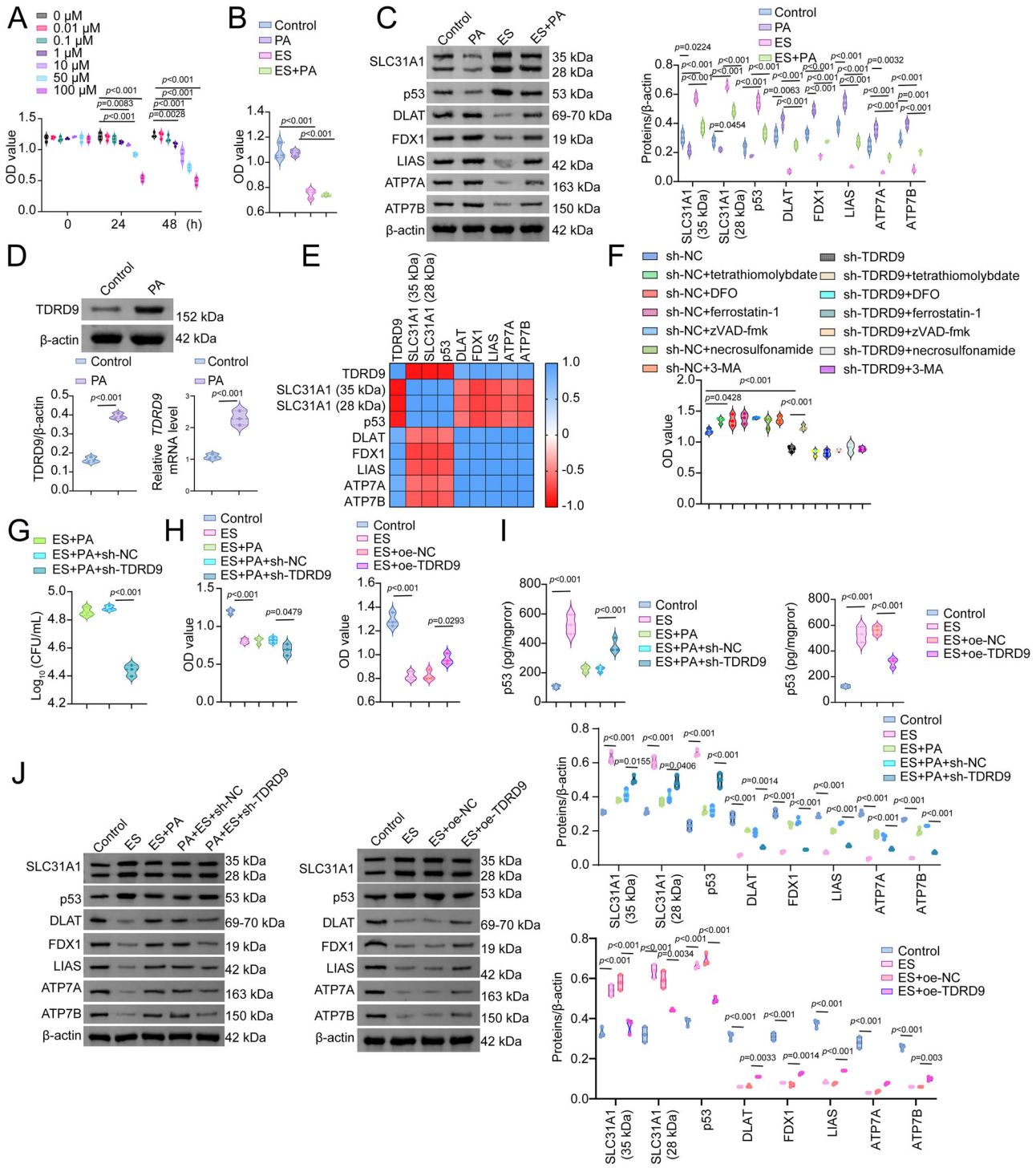

samples identified TDRD9 as a pivotal regulator of neutrophil homeostasis during PA-driven pneumonia progression. Under infection conditions, neutrophils exhibited suppressed cuproptosis in vitro and in vivo, concurrent with marked TDRD9 upregulation and exacerbated pulmonary inflammation. By employing lentiviral vectors and HA-functionalized self-assembling NPs, we achieved targeted *TDRD9* silencing, demonstrating that TDRD9 knockdown induces neutrophil cuproptosis via PD-L1/CD80/MAPK pathway inhibition, thereby attenuating PA-driven pneumonia. Validation using HLO models confirmed that HA-si-TDRD9 NPs effectively suppress bacterial growth and mitigate PA-induced HLO damage (Fig. 10). These findings establish HA-si-TDRD9 NPs as a promising targeted therapy for PA-associated pneumonia.

Neutrophil homeostasis is essential for resolving pulmonary inflammation[42]. As the predominant circulating leukocytes and first responders to pathogens, neutrophils eliminate microbes through diverse effector mechanisms while coordinating broader immune activation[43]. Aligning with prior reports[24], we observed PA-induced neutrophilic lung infiltration, a necessary defense response. However, dysregulated neutrophil activation exacerbates tissue damage via cytotoxic mediator release[44]. Infection disrupts neutrophil homeostasis, promoting cell death—apoptosis, necroptosis, pyroptosis, autophagy, and NETosis[45]—with impaired death pathways amplifying inflammation[46]. Our work revealed that PA suppresses neutrophil apoptosis, necroptosis, autophagy, and ferroptosis, while uniquely restricting copper ionophore ES-induced

https://doi.org/10.1038/s41467-026-70349-8

Fig. 5 | Tudor domain-containing protein 9 (TDRD9) suppresses neutrophil cuproptosis in vitro. A Neutrophils were pretreated with escalating doses of the copper ionophore elesclomol (ES) or dimethyl sulfoxide (DMSO; vehicle control) for 24 h. Dose-dependent cytotoxicity of ES in human neutrophils. $n = 3$ independent experiments. **B** Neutrophils were pretreated with 10 μM ES for 24 h and challenged with *Pseudomonas aeruginosa* (PA) strain PAO1 at a multiplicity of infection (MOI) of 10 for 1 h. Viability of neutrophils treated with 10 μM ES ± PAO1 infection. $n = 3$ independent experiments. **C** Western blot analysis of cuproptosis-related proteins under PAO1/ES co-treatment. $n = 3$ independent experiments. **D** PAO1-induced TDRD9 upregulation. $n = 3$ independent experiments. **E** Correlation heatmap between TDRD9 and cuproptosis regulators. **F** Neutrophils were pre-transducted with lentiviral-based short hairpin RNA (shRNA) knocking down Tudor domain-containing protein 9 (*TDRD9*) (sh-TDRD9) and exposed to 20 μM tetrathiomolybdate (cuproptosis inhibitor; 2 h), 50 μM deferoxamine (DFO; iron chelator; 1 h), 10 μM ferrostatin-1 (ferroptosis inhibitor; 1 h), 5 μM Z-VAD-FMK (pan-caspase inhibitor; 1 h), 1 μM necrosulfonamide (necroptosis inhibitor; 1 h), and 500 μM 3-methyladenine (3-MA; autophagy inhibitor; 1 h). Neutrophil viability under pharmacological inhibition of alternative cell death pathways. $n = 3$ independent experiments. **G** Neutrophils were pre-transducted with sh-TDRD9, followed by treatment with 10 μM ES and PAO1. Quantitative analysis of colony-forming unit (CFU) in neutrophils. $n = 3$ independent experiments. **H** Neutrophils were pre-transducted with sh-TDRD9 or lentiviral TDRD9 overexpression construct (oe-TDRD9), followed by treatment with 10 μM ES and PAO1. Viability of PAO1/ES-treated neutrophils with TDRD9 knockdown/overexpression. $n = 3$ independent experiments. **I** Enzyme-linked immunosorbent assay (ELISA) analysis of tumor protein p53 (p53) levels in cell culture medium. $n = 3$ independent experiments. **J** Protein expression dynamics of cuproptosis mediators under genetic TDRD9 modulation. $n = 3$ independent experiments. Data represent median ± interquartile range (IQR), and analyzed by two-sided two-way ANOVA with Tukey's multiple comparisons test (**A**), or two-sided one-way ANOVA with Tukey's multiple comparisons test (**B**–**D**, **F**–**J**). Source data are provided as a Source Data file.

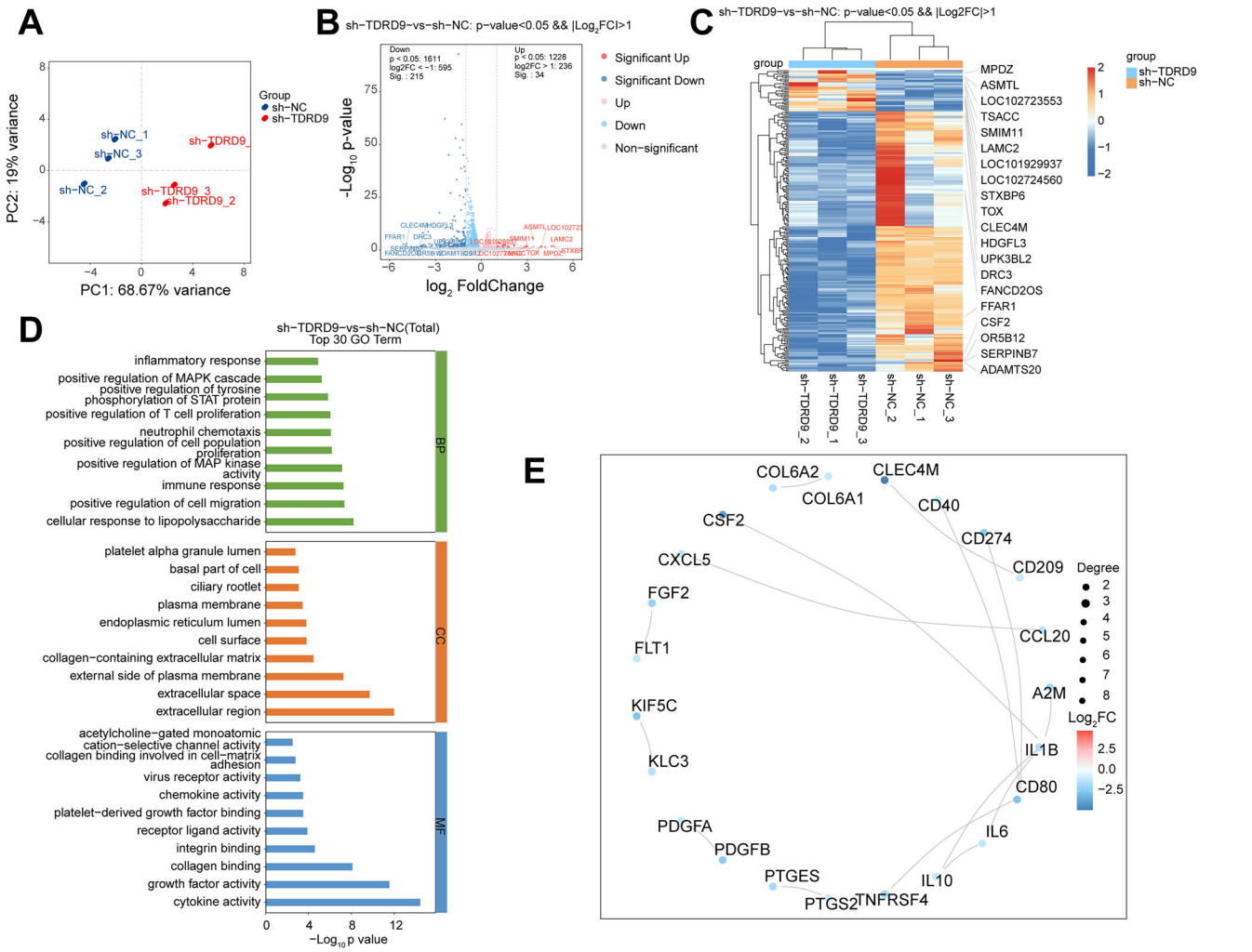

Fig. 6 | Transcriptomic landscape of Tudor domain-containing protein 9 (TDRD9)-regulated pathways in human neutrophils. A Human peripheral blood neutrophils were pre-transducted with lentiviral-based short hairpin RNA (shRNA) knocking down *TDRD9* (sh-TDRD9) or corresponding negative control vectors (sh-NC), followed by treatment with *Pseudomonas aeruginosa* (PA) strain PAO1 at a multiplicity of infection (MOI) of 10 for 1 h. RNA-sequencing on PAO1-exposed neutrophils following TDRD9 knockdown. Principal component analysis (PCA) of transcriptional profiles from sh-TDRD9 versus sh-NC neutrophils. **B** Volcano plot visualizing differentially expressed genes (DEGs) (red: upregulated; blue: down-regulated). **C** Hierarchical clustering of DEGs. **D** Gene ontology (GO) enrichment across biological processes, cellular components, and molecular functions. **E** STRING database-derived protein-protein interaction (PPI) network. Source data are provided as a Source Data file.

cuproptosis in vitro. Copper is essential for bactericidal activity[47,48] but pathogenic at elevated concentrations, where it drives cytokine storms and tissue injury[49]. Consequently, precise regulation of pulmonary copper homeostasis and neutrophil death mechanisms is critical to balancing pathogen clearance and inflammatory containment.

RNA-seq and validation across models identified TDRD9 and the PD-L1/CD80/MAPK signaling axis as critical mediators of pneumonia

https://doi.org/10.1038/s41467-026-70349-8

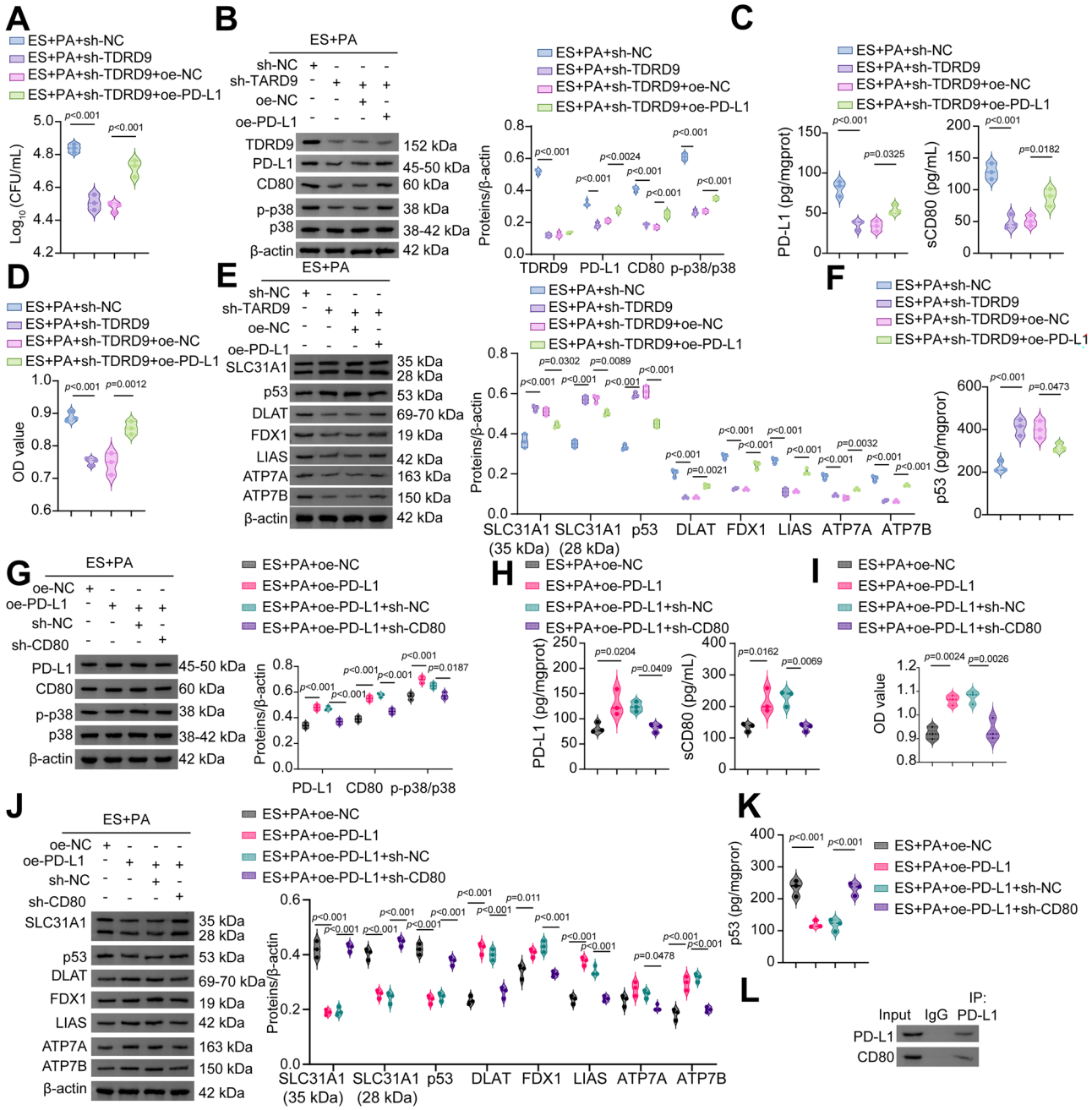

Fig. 7 | The programmed death ligand-1(PD-L1)/cluster of differentiation 80 (CD80)/mitogen-activated protein kinase (MAPK) axis mediates Tudor domain-containing protein 9 (TDRD9)-dependent cuproptosis regulation. **A** Neutrophils were pre-transducted with lentiviral-based short hairpin RNA (shRNA) knocking down *TDRD9* (sh-TDRD9) and lentiviral PD-L1 overexpression construct (oe-PD-L1), followed by treatment with 10 μM elesclomol (ES) for 24 h and *Pseudomonas aeruginosa* (PA) strain PAO1 at a multiplicity of infection (MOI) of 10 for 1 h. Quantitative analysis of colony-forming unit (CFU) in neutrophils. $n = 3$ independent experiments. **B** PD-L1 overexpression rescued TDRD9 knockdown-induced pathway suppression. $n = 3$ independent experiments. **C** Enzyme-linked immunosorbent assay (ELISA) analysis of PD-L1 and sCD80 levels in cell culture medium. $n = 3$ independent experiments. **D** Viability restoration by PD-L1 overexpression in TDRD9-depleted neutrophils. $n = 3$ independent experiments. **E** Cuproptosis-related protein dynamics under TDRD9 knockdown ± PD-L1 overexpression. $n = 3$ independent experiments. **F** ELISA analysis of tumor protein p53 (p53) levels in cell culture medium. $n = 3$ independent experiments. **G** Neutrophils were pre-transducted with oe-PD-L1 and lentiviral-based shRNA knocking down CD80 (sh-CD80), followed by treatment with 10 μM elesclomol (ES) for 24 h and infection with PAO1 at an MOI of 10 for 1 h. Signaling pathway-related protein expressions under PD-L1 overexpression ± CD80 knockdown. $n = 3$ independent experiments. **H** ELISA analysis of PD-L1 and sCD80 levels in cell culture medium. $n = 3$ independent experiments. **I** Viability reduction by CD80 knockdown in PD-L1-overexpressed neutrophils. $n = 3$ independent experiments. **J**, **K** Cuproptosis-related protein dynamics under PD-L1 overexpression ± CD80 knockdown. $n = 3$ independent experiments. **L** PD-L1-CD80 interaction using co-immunoprecipitation assay. $n = 3$ independent experiments. Data represent median ± interquartile range (IQR), and were analyzed by two-sided one-way ANOVA with Tukey's multiple comparisons test (**A**–**K**). Source data are provided as a Source Data file.

https://doi.org/10.1038/s41467-026-70349-8

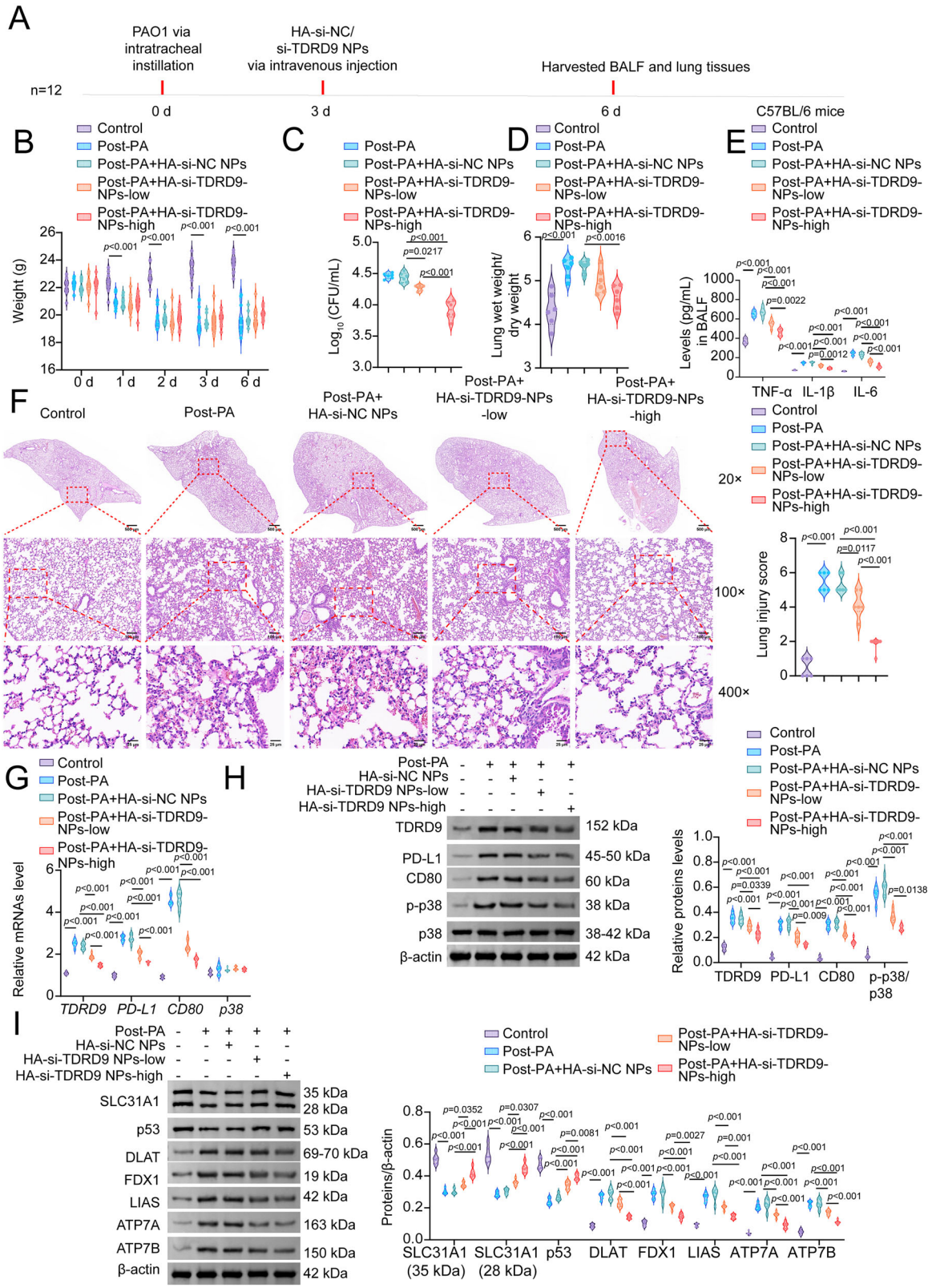

pathogenesis. The pronounced upregulation of *TDRD9* in neutrophils from PA-pneumonia patients prompted a mechanistic investigation. Neutrophil depletion via anti-Ly6G antibodies, followed by adoptive transfer of TDRD9-knockdown neutrophils, significantly attenuated pulmonary inflammation. Although TDRD9—a Tudor domain protein implicated in male germ cell development[50] and immune cell infiltration[51]—has been minimally studied in neutrophil survival, our data reveal its potential regulatory role. In vitro TDRD9 silencing reduced neutrophil viability, an effect rescued by the cuproptosis inhibitor tetrathiomolybdate but unaffected by inhibitors of apoptosis, necroptosis, autophagy, or ferroptosis, indicating TDRD9 ablation specifically triggers neutrophil cuproptosis.

This phenotype mechanistically links to PD-L1/CD80/MAPK pathway suppression. PD-L1, a key immune checkpoint, inhibits post-

Fig. 8 | HA-si-TDRD9 NPs ameliorate *Pseudomonas aeruginosa* (PA)-induced lung injury and modulate neutrophil cuproptosis. A An experimental flowchart illustrating intravenous injections of low-dose (0.1 μmol) or high-dose (0.2 μmol) hyaluronic acid (HA)-coated peptide nanoparticle (NP) system for targeted small interfering RNA (siRNA) delivery against Tudor domain-containing protein 9 (*TDRD9*) (HA-si-TDRD9 NPs) three days after PA strain PAO1 (OD_{600} = 0.6; 7×10^6 CFU/mL in 0.9% sterile saline) infection. **B** Body weight dynamics in PAO1-infected mice treated with HA-si-NC NPs or HA-si-TDRD9 NPs (0.1/0.2 μmol). $n = 12$ mice per group. **C** Quantitative analysis of colony-forming unit (CFU) in lung tissues. n = 6 mice per group. **D** Lung edema quantification via wet-to-dry weight ratios. $n = 6$ mice per group. **E** Bronchoalveolar lavage fluid (BALF) cytokine levels. $n = 6$ mice per group. **E** *TDRD9* mRNA expression in lung tissue. $n = 6$ mice per group. **F** Representative hematoxylin and eosin (HE)-stained lung images. Scale bar: 500 μm (top), 100 μm (middle), 25 μm (bottom). $n = 6$ mice per group. **G**, **H** Programmed death ligand-1(PD-L1)/cluster of differentiation 80 (CD80)/mitogen-activated protein kinase (MAPK) signaling pathway-related indicators in lung neutrophils. $n = 6$. **I** Cuproptosis-related protein expression in lung neutrophils. $n = 6$ mice per group. Data represent median ± interquartile range (IQR), and analyzed by two-sided two-way ANOVA with Tukey's multiple comparisons test (**B**), or two-sided one-way ANOVA with Tukey's multiple comparisons test (**B**–**D**, **C**–**I**). Source data are provided as a Source Data file.

infection neutrophil apoptosis and autophagy to prolong inflammatory responses[52,53]. Paradoxically, neutrophil-specific PD-L1 overexpression increases PA susceptibility, which may be attributed to impaired phagocytic capacity[54]. CD80 synergizes with PD-L1 on antigen-presenting cells to potentiate neutrophil activation[55], while MAPK signaling governs NETosis-associated pyroptosis and ferroptosis in PA-induced lung injury[56]. We demonstrated that TDRD9 knockdown suppresses PD-L1/CD80/p38 MAPK activation, thereby enabling cuproptosis.

NP-based siRNA delivery systems offer precision targeting for inflammatory lung diseases[57]. By silencing disease-promoting genes, siRNA-loaded NPs mitigate PA-induced lung injury[58]. NP systems prevent the release of toxic drugs in neutrophils and alleviate inflammation[59] and leverage peptide-based carriers for enhanced biocompatibility[60]. Utilizing HA-functionalized p5RHH-si-TDRD9 NPs, we achieved neutrophil-specific TDRD9 silencing in vitro and in vivo. HA-si-TDRD9 NPs restored pulmonary homeostasis by inducing neutrophil cuproptosis, reducing pathological neutrophil infiltration, and alleviating edema.

Compared to 2D cell cultures and animal models, 3D lung organoids exhibit superior physiological relevance to human systems, demonstrating significant potential for studying bacterial pneumonia[40,61]. Organoids circumvent batch variability issues inherent in animal studies, and a single human tissue sample can generate >100 organoids, substantially reducing inter-individual variability while enabling high-throughput screening. Organoid cultures permit precise control of pathogen exposure and drug treatment, eliminating confounding systemic factors present in animal models. This approach provides a robust platform to implement the 3 R principles—Replacement, Reduction and Refinement—in preclinical research, thereby reducing reliance on experimental animals and associated ethical concerns. Crucially, stem/progenitor cells within lung organoids exhibit self-renewal and differentiation capacities unattainable in conventional cell lines. In this study, HLOs were established via differentiation of adjacent non-cancerous lung tissues. PA exposure was demonstrated to induce apoptosis and a pro-inflammatory microenvironment in these organoids. Consistent with observations in neutrophil cultures and mouse models, HA-si-TDRD9 NPs attenuated HLO susceptibility to PA infection, mitigating apoptosis and tissue damage. These findings position HA-si-TDRD9 NPs as a targeted strategy to resolve dysregulated inflammation via cuproptosis-driven neutrophil clearance.

While this work provides some insights, certain limitations warrant consideration. First, modest cohort size restricts our ability to fully characterize dynamic microenvironmental changes during PA lung infection. A neutrophil-specific TDRD9 knockout mouse model would more rigorously delineate its regulatory role. Second, although we quantified immune cell flux in PA-infected lungs, the upstream drivers of this redistribution remain unexplored. Future investigations should address TDRD9's influence on PA virulence determinants—adhesion factors and biofilm formation—and its interplay with copper homeostasis under pathological conditions. Future establishment of airway epithelial organoids to investigate inter-individual variations in infection susceptibility and responses would strengthen mechanistic studies of PA-induced lung injury. Nanoparticle bactericidal efficacy will be validated through CFU counts in human saliva, PA-specific fluorescent imaging, and PCR detection of outer membrane protein L (*oprL*) gene expression, thereby enhancing clinical translatability. Long-term toxicity of HA-si-TDRD9 NPs was not systematically evaluated in this study, necessitating in-depth investigation of in vivo nanoparticle trafficking pathways in future research. Future studies should further explore neutrophil functional heterogeneity and the precise regulatory mechanisms of cuproptosis in infectious lung injury. The potential implications of gender as a factor in PA-induced lung injury warrant further investigation.

In conclusion, our findings position TDRD9 as a promising adjuvant therapeutic target for PA-associated lung injury. We developed a peptide-based NP platform capable of efficient TDRD9 siRNA delivery to lung neutrophils. TDRD9 silencing suppressed PD-L1/CD80/MAPK signaling, inducing neutrophil cuproptosis and attenuating PA-driven pulmonary hyperinflammation. These results underscore the therapeutic potential of HA-si-TDRD9 NPs in managing bacterial pneumonia-related immunopathology, offering a targeted strategy to restore neutrophil homeostasis.

Methods

Study approval and ethics statements

The human research protocol received ethical approval from the Biomedical Research Ethics Committee of the University of South China (Approval No. 2024077 and 2024107), with written informed consent obtained from all participants. All animal experiments were conducted in strict compliance with the National Institutes of Health Guide for the Care and Use of Laboratory Animals and were reviewed by the Biomedical Research Ethics Committee of the University of South China (Approval No. 2024-491).

Study population and sample collection

This study enrolled 15 non-pneumonia patients requiring bronchoscopy (Control), 15 patients with non-PA pneumonia (Non-PA-pneumonia), and 15 patients with PA-induced pneumonia (PA-pneumonia) at the Second Affiliated Hospital, University of South China, between March 2023 and March 2024. Patients who are pregnant or breastfeeding, have severe underlying medical conditions, are in an immunosuppressed state, are currently receiving antibiotic therapy, or have chronic respiratory failure are excluded. Based on biological attributes, each cohort includes eight males and seven females. All patient characteristics were obtained at the time of initial diagnosis (Supplementary Table 1). During standard diagnostic bronchoscopy, sterile saline was instilled into the right middle lobe or left upper lobe lingula via the bronchoscope channel, achieving a fluid recovery rate of 60–70%. Polymorphonuclear neutrophils (PMNs) were isolated from bronchoalveolar lavage fluid (BALF) and peripheral blood samples using Percoll density gradient centrifugation. Seven control subjects, eight non-PA pneumonia patients, and six pneumonia patients were randomly selected for BALF collection. The baseline information of these subjects is shown in Supplementary Table 2. BALF-derived

https://doi.org/10.1038/s41467-026-70349-8

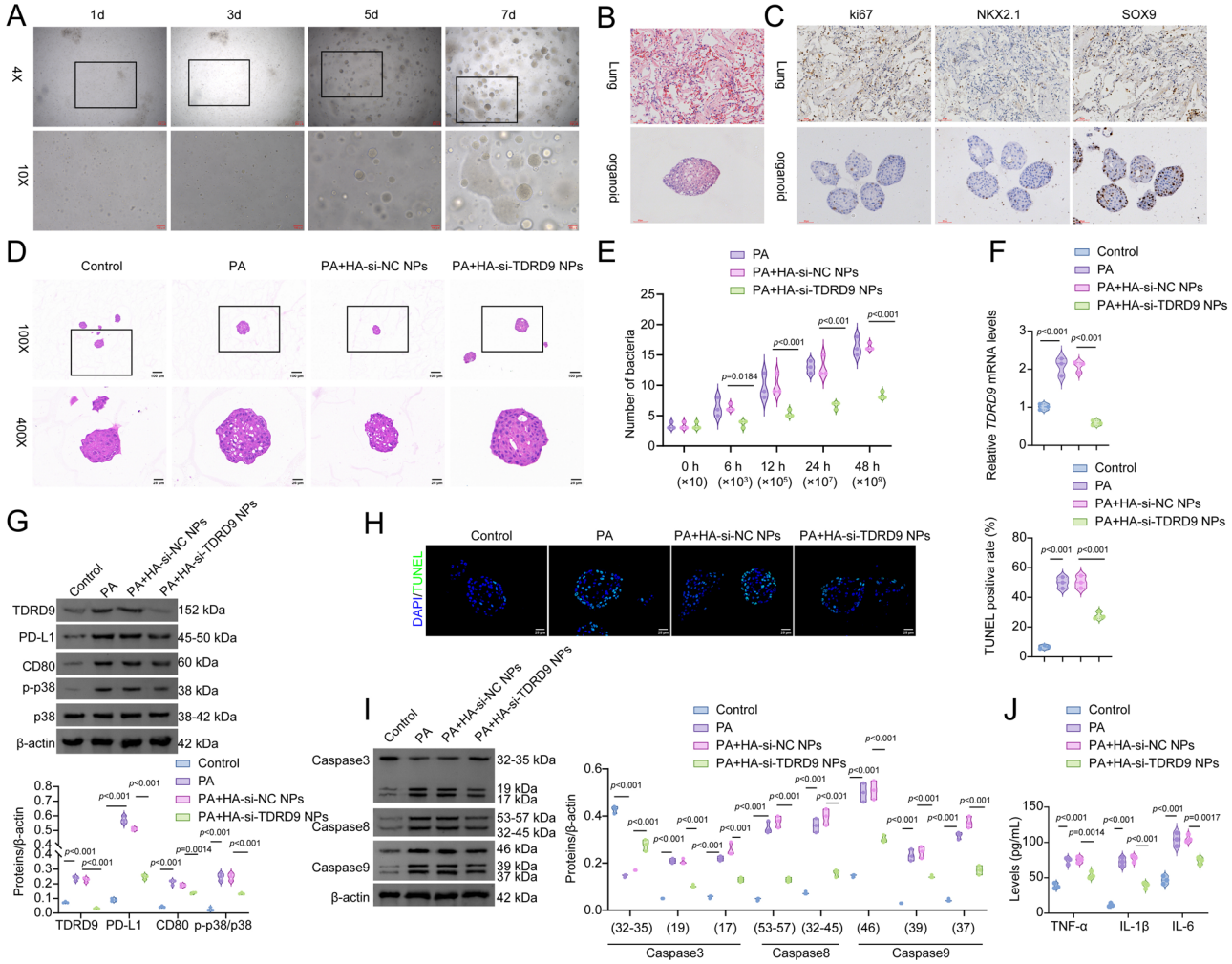

Fig. 9 | HA-si-TDRD9 NPs reduce HLO susceptibility to PA infection. A A spherical 3D human lung organoid (HLO) structure was successfully established in Matrigel, and its growth was observed under an optical microscope for 7 days. Representative bright-field images of HLOs cultured for 7 days. Scale bars: 200 μm (top), 100 μm (bottom). $n = 3$ independent experiments. **B** Hematoxylin and eosin (HE) staining comparing histological features of native human lung tissue and HLOs. Scale bar: 60 μm. $n = 3$ independent experiments. **C** Immunohistochemistry analysis of Ki67, NK2 homeobox 1 (NKX2.1), and SRY-box transcription factor 9 (SOX9) expression in native lung tissue and HLOs. Scale bar: 60 μm. $n = 3$ independent experiments. **D** HLOs were incubated with 0.1 μM hyaluronic acid (HA)-coated peptide nanoparticle (NP) system for targeted small interfering RNA (siRNA) delivery against Tudor domain-containing protein 9 (*TDRD9*) (HA-si-TDRD9 NPs) or HA-si-NC NPs, followed by infection with *Pseudomonas aeruginosa* (PA) strain PAO1. HE staining showing HA-si-TDRD9-mediated preservation of HLO morphology following PA challenge. $n = 3$ independent experiments. **E** Bacterial growth curves in HLO cultures. $n = 3$. **F** Quantitative real-time PCR analysis of *TDRD9* mRNA levels in HLOs. $n = 3$ independent experiments. **G** Western blot analysis of TDRD9, programmed death ligand-1(PD-L1), cluster of differentiation 80 (CD80), and mitogen-activated protein kinase (MAPK) expression. $n = 3$ independent experiments. **H** TUNEL assay quantifying apoptotic cells in HLOs. Scale bar: 25 μm. $n = 3$ independent experiments. **I** Western blot of cleaved caspase-3, -8, and -9 levels. $n = 3$ independent experiments. **J** Enzyme-linked immunosorbent assay (ELISA) quantification of tumor necrosis factor-alpha (TNF-α), interleukin-1 beta (IL-1β), and IL-6 levels in HLO supernatants. $n = 3$ independent experiments. Data represent median ± interquartile range (IQR), and analyzed by two-sided two-way ANOVA with Tukey's multiple comparisons test (**E**), or two-sided one-way ANOVA with Tukey's multiple comparisons test (**F**–**J**). Source data are provided as a Source Data file.

neutrophils were processed for RNA sequencing (RNA-seq), while peripheral blood neutrophils were utilized for functional in vitro assays. Human materials for organoid generation originated from adjacent non-cancerous lung tissues of three lung adenocarcinoma patients (Supplementary Table 3).

Cell culture and treatment

Isolated neutrophils were cultured in RPMI 1640 at 37 °C with 5% CO_2. Cell viability, confirmed by Ly6G/CD11b dual-labeling flow cytometry (A00-1-1102, Beckman Coulter, Fullerton, CA, USA), exceeded 95%. Neutrophils were pretreated with escalating doses of the copper ionophore elesclomol (ES) or dimethyl sulfoxide (DMSO; vehicle control) and challenged with PA strain PAO1 (ATCC #27853) at a multiplicity of infection (MOI) of 10 for 1 h[62]. For genetic manipulation, neutrophils were transducted with lentiviral-based short hairpin RNA (shRNA) knocking down *TDRD9* (sh-TDRD9; 5′-TGGCAA-TAAGTCTCATGTATT-3′, LV-HO153046-sh, HonorGene), lentiviral TDRD9 overexpression construct (oe-TDRD9; LV-HO153046, HonorGene), lentiviral PD-L1 overexpression construct (oe-PD-L1; LV-HO014143, HonorGene), lentiviral-based shRNA knocking down CD80 (sh-CD80; 5′-CCTTAATCTCAGTAAATGGAA-3′, LV-HO005191-sh, HonorGene), and their corresponding negative control vectors (NC).

Prior to bacterial challenge, cells were incubated with 10 nM U-46199 (p38 MAPK agonist) for 24 h[63]. To delineate TDRD9's role, neutrophils subjected to sh-TDRD9 were exposed to 20 μM tetrathiomolybdate (cuproptosis inhibitor; 2 h), 50 μM deferoxamine (DFO;

https://doi.org/10.1038/s41467-026-70349-8

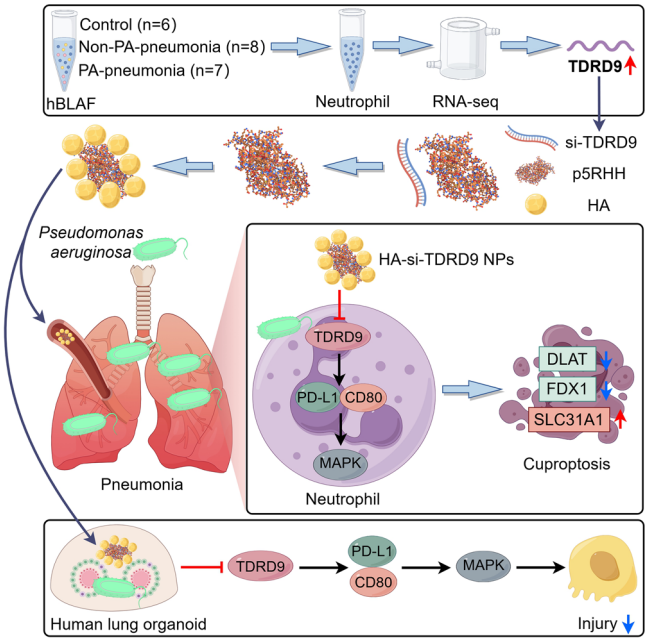

Fig. 10 | A graphic abstract summarizes that HA-si-TDRD9 NPs attenuate *Pseudomonas aeruginosa* (PA)-driven lung injury. Pathogenic gene Tudor domain-containing protein 9 (*TDRD9*) was identified through RNA sequencing of neutrophils collected from bronchoalveolar lavage fluid (BALF) of 21 recruited patients. *TDRD9*-targeting siRNA was encapsulated into hyaluronic acid (HA)-coated amphiphilic peptide p5RHH nanoparticles (NPs). Administration of HA-si-TDRD9 nanoparticles to PA-infected mice or human lung organoids demonstrated that these NPs disrupt the programmed death ligand-1(PD-L1)/cluster of differentiation 80 (CD80)/mitogen-activated protein kinase (MAPK) signaling pathway, promote neutrophil cuproptosis, and ultimately ameliorate inflammation and lung injury.

iron chelator; 1 h), 10 μM ferrostatin-1 (ferroptosis inhibitor; 1 h), 5 μM Z-VAD-FMK (pan-caspase inhibitor; 1 h), 1 μM necrosulfonamide (necroptosis inhibitor; 1 h), and 500 μM 3-methyladenine (3-MA; autophagy inhibitor; 1 h).

Cell counting kit-8 (CCK-8)

Cell viability was quantified using the CCK-8 assay (Dojindo Laboratories, Tokyo, Japan). Briefly, 100 μL of neutrophil suspension (5.5×10^3 cells/well) was seeded into 96-well plates. Following a 4-h incubation (37 °C, 5% CO_2), 100 μL of complete medium containing 10% CCK-8 reagent was added to each well. Absorbance at 450 nm (OD_{450}) was measured using a Bio-Tek Microplate Reader (HEALES, Shenzhen, China).

RNA sequencing (RNA-seq)

RNA sequencing and bioinformatic analyses were conducted by Shanghai OE Biotech Co., Ltd. (Shanghai, China). Neutrophils isolated from human subjects were subjected to RNA-seq. Sequencing reads were aligned to the human reference genome using HISAT2 (v2.1.0). Read quantification was performed with HTSeq-count (v0.11.2). Differential gene expression analysis and visualization were carried out using DESeq2 (v1.22.2) with significance thresholds set at |log2(fold change)| >1 and an adjusted p-value < 0.05. Volcano plots and heatmaps were generated to illustrate the distribution of differentially expressed genes (DEGs). Gene Ontology (GO) enrichment analysis was employed to annotate the biological functions of DEGs. Protein-protein interaction networks were constructed using the STRING database, and the top 30 interactions were visualized as circular diagrams.

Preparation and characterization of hyaluronic acid-coated p5RHH-si-TDRD9 NPs

Hyaluronic acid (HA)-coated and uncoated p5RHH-si-TDRD9 NPs were synthesized[64]. Briefly, small interfering RNA targeting TDRD9 (si-TDRD9; 10 μM) or its negative control (si-NC) was mixed with 10 mM p5RHH peptide (VLTTGLPALISWIRRRHRRHC; Cat# SC1848, GenScript, Piscataway, NJ, USA) to facilitate self-assembly of p5RHH-siRNA NPs. HA-coated NPs (HA-si-TDRD9 NPs and HA-si-NC NPs) were prepared by incubating HA solution (10 mg; Cat# B8382, ApexBio, Houston, TX, USA) with pre-assembled p5RHH-siRNA NPs. Uncoated NPs (si-TDRD9 NPs and si-NC NPs) were generated by omitting HA. Nanoparticle size and morphology were assessed by transmission electron microscopy (TEM). Hydrodynamic diameter was determined via dynamic light scattering (DLS; Zetasizer Nano ZS90, UK). si-TDRD9 (sense: 5′-UGGCAAUAAGUCUCAUGUATT-3′, antisense: 5′-UACAUGAGACUUAUUGCCATT-3′) and si-NC (sense: 5′-UUCUCCGAACGUGUCACGUTT-3′, antisense: 5′-ACGUGACACGUUCGGAGAATT-3′) were obtained from HonorGene.

Uptake of p5RHH-siRNA NPs by neutrophils

Neutrophils were seeded into 12-well plates at a density of 5×10^5 cells per well. After overnight adherence, cells were incubated with Cy5.5-labeled HA-si-TDRD9 NPs or naked si-TDRD9 NPs (HA omitted) for 4 h. Nanoparticle uptake was assessed by flow cytometry and immunofluorescence analysis of Cy5.5 and LY6G staining. To evaluate HA-mediated uptake, neutrophils were stained with anti-CD44 antibody (Cat# MU310, BioGenex, Fremont, CA, USA), followed by incubation with HA-si-TDRD9 NPs.

Animal model of pneumonia

A total of 286 male C57BL/6 mice (6–8 weeks old) were obtained from Hunan Slake Jingda Animal Experiment Company (Changsha, China) and housed at 22–26 °C with 40–60% humidity under a 12-h light/dark cycle. After mice were anesthetized via intraperitoneal injection of sodium pentobarbital (50 mg/kg), 50 μL of bacterial suspension of PAO1 ($OD_{600} = 0.6$; 7×10^6 CFU/mL in 0.9% sterile saline) was administered via oropharyngeal intratracheal instillation to simulate PA pneumonia[62]. Control mice received an equal volume of sterile saline.

Seventy-eight mice were randomly allocated to Control and PA groups ($n = 39$ per group). Three PA-group mice died during the seven-day infection period. On day 1 post-infection, twelve mice per group were randomly selected as Control-1d and PA-1d subgroups ($n = 12$ each). On day 3, twelve additional mice per group were randomly chosen from the same cohort as Control-3d and PA-3d subgroups ($n = 12$ each). The remaining mice were maintained until day 7, with 12 surviving PA-group mice designated as PA-7d and twelve randomly selected Control-group mice as Control-7d ($n = 12$ each). Euthanasia was performed via sodium pentobarbital overdose (100 mg/kg). Six mice per subgroup underwent pulmonary edema evaluation. From the remaining six mice per subgroup, BALF was collected through lung lavage with 1 mL ice-cold phosphate-buffered saline (PBS), while peripheral blood and lung tissues were harvested for downstream analyses.

To investigate the in vivo role of TDRD9 in neutrophils, seventy-eight mice were randomly allocated to six experimental groups: Control, Anti-Ly6G, PA, Anti-Ly6G+PA, Anti-Ly6G+PA+$PMN^{sh\text{-}NC}$, and Anti-Ly6G+PA+$PMN^{sh\text{-}TDRD9}$ ($n = 12$ per group). Mice in anti-Ly6G-treated groups were intravenously administered 50 μg anti-Ly6G antibody 48 h prior to PAO1 infection to deplete endogenous neutrophils[65]. Neutrophils (1×10^6 cells/mouse) transducted with sh-TDRD9 (5′-AGCTCAGAAATGGAGTATATT-3′, LV-MO029056-sh, HonorGene) or sh-NC were adoptively transferred via intravenous injection[66]. Control mice received equivalent volumes of sterile saline. On day 3, BALF and lung tissues were collected for further evaluation.

In vitro and in vivo targeting efficacy of HA-p5RHH-siRNA NPs

The regulatory effects of HA-si-TDRD9 NPs on the PD-L1/CD80/MAPK signaling axis and cuproptosis were assessed. Human peripheral blood neutrophils were incubated with 0.1 μM HA-si-NC NPs or HA-si-TDRD9 NPs for 4 h[64]. Neutrophils were subsequently treated with 10 μM ES for 24 h, followed by infection with PAO1 for 1 h. For PD-L1 overexpression, neutrophils were transfected with oe-PD-L1 or oe-NC. Prior to bacterial challenge, cells were pre-treated with 1 μM SB203580 (p38 MAPK inhibitor) for 1 h[56,67].

The therapeutic efficacy of HA-si-TDRD9 NPs was evaluated in mice. Sixty-five mice were randomly allocated to five experimental groups: Control, Post-PA, Post-PA + HA-si-NC NPs, Post-PA + HA-si-TDRD9 NPs-low, and Post-PA + HA-si-TDRD9 NPs-high ($n = 12$ per group). Mice received intravenous injections of low-dose (0.1 μmol) or high-dose (0.2 μmol) HA-si-TDRD9 nanoparticles three days post-infection. Body weight was monitored daily for six consecutive days post-infection, with BALF and lung tissue samples collected on day 3 post-treatment.

To evaluate the preventive protective effects of HA-si-TDRD9 NPs, 65 mice were randomly allocated to five experimental groups: Control, Pre-PA, Pre-PA + HA-si-NC NPs, Pre-PA + HA-si-TDRD9 NPs-low, and Pre-PA + HA-si-TDRD9 NPs-high ($n = 12$ per group). Mice received intravenous injections of HA-si-TDRD9 NPs at low (0.1 μmol) or high (0.2 μmol) doses[64] 24 h pre-infection, with subsequent doses administered every 48 h. Body weight changes were monitored for 3 days post-infection. BALF and lung tissues were harvested on day 3.

Organoid culture

Fresh adjacent non-cancerous lung tissue samples from patients were collected and preserved in tissue preservation solution (Cat# OGCP-04-06, Guangzhou Wogen Biotechnology Co., Ltd., Guangzhou, China) at 4 °C. The tissues were minced into 1–2 mm^3 fragments using surgical scissors in PBS containing 1% penicillin–streptomycin. Fragments were digested with organoid digestion solution (Cat# OGCP-04-01) for 1–2 h, filtered through a 100 μm cell strainer, and pelleted by centrifugation. The pellet was resuspended in Matrigel (Cat# OGCP-04-11) mixed 1:1 with organoid culture medium (Cat# OGCP-02-07). A 50 μL aliquot of the mixture was plated and solidified at 37 °C under 5% CO_2, followed by the addition of 500 μL organoid culture medium. Organoid growth was monitored daily for 7 days, with medium replaced every 2–3 days.

Bacterial growth assay

For bacterial inoculation, organoid culture medium, cells, and lung tissue homogenate were combined with sterile PBS and spiked with PA at an initial concentration of ~3×10^2 CFU/mL. A 100 μL aliquot of the mixture was seeded into LB medium and incubated at 37 °C with 5% CO_2 for 6, 12, 24, and 48 h. Bacterial colonies were visualized, and colony-forming units (CFU) were quantified at each timepoint.

Lung water content

Lung edema was quantified using the wet/dry weight ratio. Immediately after euthanasia, the lungs were exercised and weighed to determine wet weight. Tissues were then dehydrated at 60 °C for 72 h in a laboratory oven until constant dry weight was achieved. The ratio of wet weight to dry weight was calculated to assess pulmonary edema severity.

Hematoxylin and eosin (HE) staining

Fresh lung, hepatic, and renal tissues from all animal groups and HLOs were fixed in 4% PFA for 24 h at 4 °C, paraffin-embedded, and sectioned at 4 μm thickness. Sections were stained with hematoxylin (Cat# AWI0001a, Abiowell) and eosin (Cat# AWI0029a, Abiowell). Histopathological damage was evaluated under a BA210T bright-field microscope (Motic, Xiamen, China) at 20×, 100×, and 400× magnification. According to established protocols[68], pneumonia severity was quantified by assessing four parameters: (1) alveolar congestion, (2) hemorrhage, (3) leukocyte infiltration, and (4) alveolar wall thickness/hyaline membrane formation (0 = absent; 3 = severe). The total score ranges from 0 to 12 points.

Flow cytometry

Lung tissues were dissociated by mincing followed by enzymatic digestion in RPMI-1640 medium containing collagenase IV and DNase I at 37 °C for 30 min. The homogenate was filtered through a 70 μm cell strainer and centrifuged at $300 \times g$ for 5 min. Red blood cells were lysed using ACK buffer, and single-cell suspensions were prepared in PBS supplemented with 2% FBS. For immunophenotyping, cells were stained for 30 min at 4 °C with the following fluorochrome-conjugated antibodies: Ly6G-PC7 (1A8-Ly6g) (Cat# 25-9668-82, eBioscience, San Diego, CA, USA), F4/80-PC5.5 (BM8) (Cat# 45-4801-82, eBioscience), CD19-APC (eBio1D3 (1D3)) (Cat# 17-0193-82, eBioscience), CD3 (145-2C11) (Cat# 12-0031-82, eBioscience), CD49b (DX5) (Cat# 11-5971-82, eBioscience). Data acquisition was performed on a CytoFLEX flow cytometer (A00-1-1102, Beckman Coulter). Neutrophils (Ly6G+), macrophages (F4/80+), B cells (CD19+), NK cells (CD49b+), and T cells (CD3+) were quantified using CytExpert v2.5 software (Beckman Coulter).

For intracellular cytokine staining, single-cell suspensions were stimulated with Cell Stimulation Cocktail (Cat# 00-4975-93, eBioscience) for 4 h at 37 °C under 5% CO_2. Cells were surface-stained with CD4 (GK1.5) (Cat# 11-0041-82, eBioscience) and intracellularly stained with: IL-17A (eBio17B7) (Cat# 12-7177-81, eBioscience), CD25 (PC61.5) (Cat# 17-0251-82, eBioscience), and Foxp3 (FJK-16s) (Cat# 12-5773-82, eBioscience). Th17 (CD4 + IL-17A+) and Treg (CD4+CD25+Foxp3+) populations were gated using CytExpert v2.5 software, and the Th17/Treg ratio was calculated.

Enzyme-linked immunosorbent assay (ELISA)

Proinflammatory cytokines (IL-6, IL-1β, TNF-α) in BALF and HLOs were quantified using commercial mouse ELISA kits (IL-6: Cat# CSB-E04639m; IL-1β: Cat# CSB-E08054m; TNF-α: Cat# CSB-E04741m; CUSABIO Co., Ltd., Wuhan, China) and human ELISA kits (IL-6: Cat# KE00139; IL-1β: Cat# KE00021; TNF-α: Cat# KE00154; Proteintech). BALF and HLO samples were centrifuged to remove cellular debris. Soluble cluster of differentiation 80 (sCD80), p53, and programmed death ligand-1(PD-L1) in cell culture medium were measured using commercial human ELISA kits (sCD80: CSB-E15768h-IS; p53: Cat# CSB-E08334h-IS; PD-L1: CSB-E13644h; CUSABIO Co., Ltd.). Assays were performed according to the manufacturer's protocol, with absorbance measured at 450 nm using a Bio-Tek microplate reader.

Quantitative real-time PCR (qRT-PCR)

Total RNA was isolated from neutrophils, lung tissues, and HLOs using TRIzol reagent (Cat# 15596026, Thermo Fisher Scientific). RNA purity and concentration were determined using a Micro Drop spectrophotometer (Thermo Fisher Scientific). Complementary DNA (cDNA) synthesis was performed with 2 μg total RNA using the HiFiScript cDNA Synthesis Kit (Cat# CW2569M, CWBIO, Taizhou, China), following the manufacturer's protocol. qRT-PCR amplification was conducted in a QuantStudio 1 Real-Time PCR System (Thermo Fisher Scientific) using UltraSYBR Mixture (Cat# CW2601M, CWBIO). Gene-specific primers (Supplementary Table 4) were designed using NCBI Primer-BLAST. Relative mRNA expression levels were calculated using the $2^{-\Delta\Delta Ct}$ method, normalized to the endogenous control *β-actin*.

Western blot analysis

Total protein was extracted from neutrophils, lung tissues, and HLOs using RIPA lysis buffer (Cat# R0010, Solarbio, Beijing, China). Equal amounts of protein were resolved on 10% SDS-polyacrylamide gels and

transferred to nitrocellulose membranes. After blocking with 5% non-fat dry milk, membranes were incubated with primary antibodies overnight at 4 °C and with horseradish peroxidase (HRP)-conjugated secondary antibodies for 1 h at room temperature (Supplementary Table 5). Immunoreactive bands were imaged on a ChemiScope 6100 imaging system (CLiNX Science Instruments, Shanghai, China) and quantified using ImageJ v1.51 software (NIH, Bethesda, MD, USA) normalized to β-actin expression.

Immunofluorescence (IF) and immunohistochemistry (IHC)

For IF, lung tissue sections were subjected to microwave-mediated antigen retrieval in Tris-EDTA buffer. Autofluorescence was quenched by incubating sections with 0.1% sodium borohydride, followed by endogenous peroxidase blockade using 0.3% hydrogen peroxide. Sections were blocked with 5% BSA and incubated with anti-LY6G (1A8) (1:200; Cat# 65078-1-Ig, Proteintech, Rosemont, IL, USA), DLAT polyclonal (1:100; Cat# 13426-1-AP, Proteintech), and FDX1 polyclonal (1:100; Cat# 12592-1-AP, Proteintech) primary antibodies and HRP-conjugated secondary antibody (1:200; Cat# AWI0629, Abiowell). Tyramide signal amplification (TSA) was performed using 520 and 570 fluorophores (Abiowell). Nuclei were counterstained with 4′,6-diamidino-2-phenylindole (DAPI). Fluorescent images were acquired using a Motic BA410 fluorescence microscope.

For IHC, dewaxed HLO sections underwent heat antigen retrieval followed by endogenous peroxidase blockade with 1% periodic acid. Tissue sections were incubated with primary antibodies against Ki67 (45b13) (1:200; Cat# AWA11025, Abiowell), NKX2.1 (EP1584Y) (1:200; Cat# ab76013, Abcam), and SOX9 (45A09) (1:200; Cat# AWA10351, Abiowell) at 4 °C overnight and species-matched HRP-conjugated secondary antibodies at 37 °C for 1 h. Sections were stained with 3,3′-diaminobenzidine (DAB) and hematoxylin. Images were captured using a bright-field microscope and analyzed using Image-Pro Plus software v6.0 (Media Cybernetics, Rockville, MD, USA).

TUNEL assay

Paraffin-embedded HLOs were dehydrated and treated with 100 µL of 1 × Proteinase K working solution. Subsequently, 100 µL of 1 × Equilibration Buffer was added and incubated at room temperature for 10–30 min, followed by the addition of 50 µL TdT incubation buffer. The samples were protected from light and incubated for 60 min. After washing with PBS, nuclei were counterstained with DAPI. Fluorescence microscopy was performed to capture images, and the percentage of TUNEL-positive cells was quantified.

Co-immunoprecipitation (Co-IP) assay

Total cellular proteins were extracted using ice-cold IP lysis buffer (Abiowell) supplemented with protease inhibitor cocktail. For immunoprecipitation, lysate was incubated overnight at 4 °C with Rabbit anti-PD-L1 (Cat# 28076-1-AP, Proteintech) or Rabbit IgG isotype control (Cat# B900610, Proteintech), followed by 4-h incubation with Protein A/G agarose beads. Beads were washed with lysis buffer, and bound proteins were eluted in IP lysis buffer. Eluates were resolved by SDS-PAGE and immunoblotted using Rabbit anti-PD-L1 and Rabbit anti-CD80 antibodies.

Detection of reactive oxygen species (ROS) and Fe^{2+} levels

Intracellular ROS levels were quantified using a CytoFLEX flow cytometer with the DCFH-DA Cellular ROS Assay Kit (Cat# S0033S, Beyotime, Shanghai, China). Fe^{2+} concentrations (µmol/10^6) were determined using the Cell Ferrous Iron Colorimetric Assay Kit (Cat# E-BC-K881-M, Elabscience, Wuhan, China).

Statistical analysis

Data are presented as mean ± standard deviation (SD). Statistical comparisons were performed in GraphPad Prism v9.0 (GraphPad Software, San Diego, CA, USA). Two-group comparisons were performed using unpaired two-sided *t*-test. Multi-group comparisons were performed using two-sided ANOVA with Tukey's post hoc test. Pearson's coefficients for TDRD9 and cuproptosis-related protein expression were analyzed. A p-value < 0.05 was considered statistically significant. All experiments were independently repeated at least three times with technical triplicates.

Reporting summary

Further information on research design is available in the Nature Portfolio Reporting Summary linked to this article.

Data availability

Source data are provided with this paper. All data generated in this study are available in the article, supplementary information, and Source Data files. The sequence data generated in this study have been submitted to the NCBI SRA database and can be accessed via the following links: https://www.ncbi.nlm.nih.gov/sra/PRJNA1297888 and https://www.ncbi.nlm.nih.gov/sra/PRJNA1299073. Source data are provided with this paper.

References

1. Faure, E., Kwong, K. & Nguyen, D. Pseudomonas aeruginosa in chronic lung infections: how to adapt within the host? *Front Immunol.* **9**, 2416 (2018).
2. Reynolds, D. & Kollef, M. The epidemiology and pathogenesis and treatment of Pseudomonas aeruginosa infections: an update. *Drugs* **81**, 2117–2131 (2021).
3. Jurado-Martín I., Sainz-Mejías M., McClean S. Pseudomonas aeruginosa: an audacious pathogen with an adaptable arsenal of virulence factors. *Int. J. Mol. Sci.* **22**, 3128 (2021).
4. Cendra, M. D. M. & Torrents, E. Pseudomonas aeruginosa biofilms and their partners in crime. *Biotechnol. Adv.* **49**, 107734 (2021).
5. Giovagnorio F., De Vito A., Madeddu G., Parisi S. G., Geremia N. Resistance in *Pseudomonas aeruginosa*: a narrative review of antibiogram interpretation and emerging treatments. *Antibiotics* **12**, 1621 (2023).
6. Wood S. J., Goldufsky J. W., Seu M. Y., Dorafshar A. H., Shafikhani S. H. Pseudomonas aeruginosa cytotoxins: mechanisms of cytotoxicity and impact on inflammatory responses. *Cells* **12**, 1621 (2023).
7. Zhou X., Jin J., Lv T., Song Y. A narrative review: the role of NETs in acute respiratory distress syndrome/acute lung injury. *Int. J. Mol. Sci.* **25**, 1464 (2024).
8. Jie, F. et al. Influenza virus infection increases host susceptibility to secondary infection with Pseudomonas aeruginosa, and this is attributed to neutrophil dysfunction through reduced myeloperoxidase activity. *Microbiol. Spectr.* **11**, e0365522 (2023).
9. Skopelja-Gardner, S. et al. Regulation of *Pseudomonas aeruginosa*-mediated neutrophil extracellular traps. *Front. Immunol.* **10**, 1670 (2019).
10. Santoni, K. et al. Caspase-1-driven neutrophil pyroptosis and its role in host susceptibility to Pseudomonas aeruginosa. *PLoS Pathog.* **18**, e1010305 (2022).
11. Tsvetkov, P. et al. Copper induces cell death by targeting lipoylated TCA cycle proteins. *Science* **375**, 1254–1261 (2022).
12. Huang, J., Zhang, J., Wang, F., Zhang, B. & Tang, X. Comprehensive analysis of cuproptosis-related genes in immune infiltration and diagnosis in ulcerative colitis. *Front. Immunol.* **13**, 1008146 (2022).
13. Ma, R., Sun, D., Wang, Y., Huang, X. & Ye, Q. Cuproptosis-associated hub gene identification and immune cell infiltration patterns in silicosis. *Toxicology* **504**, 153762 (2024).
14. Yi N., Zhang L., Huang X., Ma J., Gao J. Lenvatinib-activated NDUFA4L2/IL33/PADI4 pathway induces neutrophil extracellular traps that inhibit cuproptosis in hepatocellular carcinoma. *Cell Oncol.* **48**, 487–504 (2024).

15. Zoulikha, M. et al. Pulmonary delivery of siRNA against acute lung injury/acute respiratory distress syndrome. *Acta Pharm. Sin. B* **12**, 600–620 (2022).
16. Cox, A., Lim, S. A. & Chung, E. J. Strategies to deliver RNA by nanoparticles for therapeutic potential. *Mol. Asp. Med.* **83**, 100991 (2022).
17. Koeppen, K. et al. Let-7b-5p in vesicles secreted by human airway cells reduces biofilm formation and increases antibiotic sensitivity of P. aeruginosa. *Proc. Natl. Acad. Sci. USA* **118**, (2021).
18. Huang, P., Li, Z., Liu, R., Bartlam, M. & Wang, Y. Polystyrene nanoparticles induce biofilm formation in *Pseudomonas aeruginosa*. *J. Hazard Mater.* **469**, 133950 (2024).
19. Arafat, M. et al. Mutation in TDRD9 causes non-obstructive azoospermia in infertile men. *J. Med. Genet.* **54**, 633–639 (2017).
20. Viz-Lasheras, S. et al. A 5-transcript signature for discriminating viral and bacterial etiology in pediatric pneumonia. *iScience* **28**, 111747 (2025).
21. Bertrams, W. et al. A mRNA panel for differentiation between acute exacerbation or pneumonia in COPD patients. *Front. Med.* **11**, 1234068 (2024).
22. Kumar, V. Pulmonary innate immune response determines the outcome of inflammation during pneumonia and sepsis-associated acute lung injury. *Front. Immunol.* **11**, 1722 (2020).
23. Wagener, B. M. et al. α-Tocopherol attenuates the severity of *Pseudomonas aeruginosa*-induced pneumonia. *Am. J. Respir. Cell Mol. Biol.* **63**, 234–243 (2020).
24. Nagre, N. et al. Activation of cannabinoid-2 receptor protects against *Pseudomonas aeruginosa*-induced acute lung injury and inflammation. *Respir. Res.* **23**, 326 (2022).
25. Tu, H. et al. Dying to defend: neutrophil death pathways and their implications in immunity. *Adv. Sci.* **11**, e2306457 (2024).
26. Hou, X. et al. Role of cuproptosis in mediating the severity of experimental malaria-associated acute lung injury/acute respiratory distress syndrome. *Parasit. Vectors* **17**, 433 (2024).
27. Voli, F. et al. Intratumoral copper modulates PD-L1 expression and influences tumor immune evasion. *Cancer Res.* **80**, 4129–4144 (2020).
28. Yan, C. et al. Inhalable metal-organic framework-mediated cuproptosis combined with PD-L1 checkpoint blockade for lung metastasis synergistic immunotherapy. *Acta Pharm. Sin. B* **14**, 2281–2297 (2024).
29. Li P., Sun Q., Bai S., Wang H., Zhao L. Combination of the cuproptosis inducer disulfiram and anti-PD-L1 abolishes NSCLC resistance by ATP7B to regulate the HIF-1 signaling pathway. *Int. J. Mol. Med.* **53**, 19 (2024).
30. Shen, Z. et al. Exploration of a screening model for intrahepatic cholangiocarcinoma patients prone to cuproptosis and mechanisms of the susceptibility of CD274-knockdown intrahepatic cholangiocarcinoma cells to cuproptosis. *Cancer Gene Ther.* **30**, 1663–1678 (2023).
31. Yan, J., Li, Z., Li, Y. & Zhang, Y. Sepsis-induced cardiotoxicity by promoting cardiomyocyte cuproptosis. *Biochem. Biophys. Res. Commun.* **690**, 149245 (2024).
32. Zhang, Y. C., Zhang, Y. T., Wang, Y., Zhao, Y. & He, L. J. What role does PDL1 play in EMT changes in tumors and fibrosis? *Front. Immunol.* **14**, 1226038 (2023).
33. Ma, M. M., Zhao, J., Liu, L. & Wu, C. Y. Identification of cuproptosis-related genes in Alzheimer's disease based on bioinformatic analysis. *Eur. J. Med. Res.* **29**, 495 (2024).
34. Lan, F., Zhao, J., Liang, D., Mo, C. & Shi, W. Comprehensive analysis of cuproptosis-related ceRNA network and immune infiltration in diabetic kidney disease. *Heliyon* **10**, e35700 (2024).
35. Wang, X. et al. Adrenomedullin/FOXO3 enhances sunitinib resistance in clear cell renal cell carcinoma by inhibiting FDX1 expression and cuproptosis. *FASEB J.* **37**, e23143 (2023).
36. Nishimura, C. D., Pulanco, M. C., Cui, W., Lu, L. & Zang, X. PD-L1 and B7-1 cis-interaction: new mechanisms in immune checkpoints and immunotherapies. *Trends Mol. Med* **27**, 207–219 (2021).
37. Kim, H., Shin, M., Han, S., Kwon, W. & Hahn, S. K. Hyaluronic acid derivatives for translational medicines. *Biomacromolecules* **20**, 2889–2903 (2019).
38. Lee, Y. et al. Hyaluronic acid-bilirubin nanomedicine-based combination chemoimmunotherapy. *Nat. Commun.* **14**, 4771 (2023).
39. Yan, H. et al. Induction of WNT16 via peptide-mRNA nanoparticle-based delivery maintains cartilage homeostasis. *Pharmaceutics* **12**, 73 (2020).
40. Vazquez-Armendariz A. I., Tata P. R. Recent advances in lung organoid development and applications in disease modeling. *J. Clin. Investig.* **133**, e170500 (2023).
41. Curran, C. S., Bolig, T. & Torabi-Parizi, P. Mechanisms and targeted therapies for Pseudomonas aeruginosa lung infection. *Am. J. Respir. Crit. Care Med.* **197**, 708–727 (2018).
42. Singhal, A. & Kumar, S. Neutrophil and remnant clearance in immunity and inflammation. *Immunology* **165**, 22–43 (2022).
43. Herro, R. & Grimes, H. L. The diverse roles of neutrophils from protection to pathogenesis. *Nat. Immunol.* **25**, 2209–2219 (2024).
44. Liew, P. X. & Kubes, P. The neutrophil's role during health and disease. *Physiol. Rev.* **99**, 1223–1248 (2019).
45. Pérez-Figueroa, E., Álvarez-Carrasco, P., Ortega, E. & Maldonado-Bernal, C. Neutrophils: many ways to die. *Front. Immunol.* **12**, 631821 (2021).
46. Zhu, C. L. et al. Dysregulation of neutrophil death in sepsis. *Front. Immunol.* **13**, 963955 (2022).
47. Hofmann L., Hirsch M., Ruthstein S. Advances in understanding of the copper homeostasis in *Pseudomonas aeruginosa*. *Int. J. Mol. Sci.* **22**, 2050 (2021).
48. O'Brien, H., Davoodian, T. & Johnson, M. D. L. The promise of copper ionophores as antimicrobials. *Curr. Opin. Microbiol.* **75**, 102355 (2023).
49. Lu, J. et al. Copper regulates the host innate immune response against bacterial infection via activation of ALPK1 kinase. *Proc. Natl. Acad. Sci. USA* **121**, e2311630121 (2024).
50. Wenda, J. M. et al. Distinct roles of RNA helicases MVH and TDRD9 in PIWI slicing-triggered mammalian piRNA biogenesis and function. *Dev. Cell* **41**, 623–637.e629 (2017).
51. Ba, H. et al. Identification of hub biomarkers and immune and inflammation pathways contributing to Kawasaki disease progression with RT-qPCR verification. *J. Immunol. Res.* **2023**, 1774260 (2023).
52. Wang, J. F. et al. Upregulated PD-L1 delays human neutrophil apoptosis and promotes lung injury in an experimental mouse model of sepsis. *Blood* **138**, 806–810 (2021).
53. Zhu, C. L. et al. PD-L1 maintains neutrophil extracellular traps release by inhibiting neutrophil autophagy in endotoxin-induced lung injury. *Front. Immunol.* **13**, 949217 (2022).
54. Luo, L. et al. Fine particulate matter 2.5 induces susceptibility to *Pseudomonas aeruginosa* infection via expansion of PD-L1(high) neutrophils in mice. *Respir. Res.* **25**, 90 (2024).
55. Pylaeva, E. et al. During early stages of cancer, neutrophils initiate anti-tumor immune responses in tumor-draining lymph nodes. *Cell Rep.* **40**, 111171 (2022).
56. Aji, N. et al. PAI-1 deficiency promotes NET-mediated pyroptosis and ferroptosis during *Pseudomonas Aeruginosa*-induced acute lung injury by regulating the PI3K/MAPK/AKT axis. *Inflammation* **48**, 1109–1124 (2024).
57. Moazzam, M. et al. The landscape of nanoparticle-based siRNA delivery and therapeutic development. *Mol. Ther.* **32**, 284–312 (2024).
58. Qin, S. et al. Pseudomonas aeruginosa: pathogenesis, virulence factors, antibiotic resistance, interaction with host, technology

advances and emerging therapeutics. *Signal Transduct. Target. Ther.* **7**, 199 (2022).
59. Chu, D., Dong, X., Shi, X., Zhang, C. & Wang, Z. Neutrophil-based drug delivery systems. *Adv. Mater.* **30**, e1706245 (2018).
60. Tan, L. et al. Peptide-based nanomaterials: self-assembly and applications. *Mini Rev. Med. Chem.* **23**, 399–411 (2023).
61. Mahieu L., Van Moll L., De Vooght L., Delputte P., Cos P. In vitro modelling of bacterial pneumonia: a comparative analysis of widely applied complex cell culture models. *FEMS Microbiol. Rev.* **48**, fuae007 (2024).
62. Sung P. S., Peng Y. C., Yang S. P., Chiu C. H., Hsieh S. L. CLEC5A is critical in *Pseudomonas aeruginosa*-induced NET formation and acute lung injury. *JCI Insight* **7**, e156613 (2022).
63. Zhang, Y., Zhu, C., Zhao, H., Sun, Z. & Wang, X. Anti-inflammatory effect of chlorogenic acid in Klebsiella pneumoniae-induced pneumonia by inactivating the p38MAPK pathway. *Int. J. Med. Microbiol.* **313**, 151576 (2023).
64. Yan, H. et al. Peptide-siRNA nanoparticles targeting NF-κB p50 mitigate experimental abdominal aortic aneurysm progression and rupture. *Biomater. Adv.* **139**, 213009 (2022).
65. Cai, W. et al. All trans-retinoic acid protects against acute ischemic stroke by modulating neutrophil functions through STAT1 signaling. *J. Neuroinflamm.* **16**, 175 (2019).
66. Pu, Q. et al. Bitter receptor TAS2R138 facilitates lipid droplet degradation in neutrophils during *Pseudomonas aeruginosa* infection. *Signal Transduct. Target Ther.* **6**, 210 (2021).
67. Wang, W. et al. Role of TLR4-p38 MAPK-Hsp27 signal pathway in LPS-induced pulmonary epithelial hyperpermeability. *BMC Pulm. Med.* **18**, 178 (2018).
68. Li, H., Li, X., Ai, Q. & Tan, L. Autoinducer-2 promotes *Pseudomonas aeruginosa* PAO1 acute lung infection via the IL-17A pathway. *Front. Microbiol.* **13**, 948646 (2022).

Acknowledgements

This work was supported by the National Natural Science Foundation of China (82200017), the Science and Technology Innovation Program of Hunan Province, China (2023RC3198), Natural Science Foundation of Hunan Province, China (2025JJ50622), Scientific Research Project of Hunan Provincial Health Commission, China (20255112) and Scientific Research Project of Hunan Provincial Education Department (25A0327). The graphical abstract (Fig. 10) was created using the open online platform Figdraw (https://www.figdraw.com/static/index.html#/; RSYTY2d253).

Author contributions

X.W.: Data curation, Formal analysis, Funding acquisition, Conceptualization, Funding acquisition, Project administration, Writing-review & editing; W.Z., H.L.: Data curation, Formal analysis, Visualization, Writing-original draft; H.J.: Data curation, Formal analysis, Visualization; L.D.: Formal analysis, Investigation; Z.T., W.X.: Methodology, Resource; Q.W., M.Z.: Data curation. All authors supervised the results, revised the manuscript, and approved the final manuscript.

Competing interests

The authors declare no competing interests.

Additional information

Supplementary information The online version contains supplementary material available at https://doi.org/10.1038/s41467-026-70349-8.

Correspondence and requests for materials should be addressed to Xu Wu.

Peer review information *Nature Communications* thanks the anonymous reviewers for their contribution to the peer review of this work. A peer review file is available.